Report

Hydrothermal Gasification of HTL wastewater

By
Jakob Breinl

Supervised by
Yuanhui Zhang, Ph.D., P.E.
The Innoventor Professor in Engineering
and the Associate Department Head,
Department of Agricultural and Biological Engineering
University of Illinois at Urbana-Champaign

Vienna, Austria
February 2015

Acknowledgement

The present work was implemented within the scope of a cooperation project between Vienna University of Technology (TU Vienna) and the University of Illinois at Urbana-Champaign (UIUC). It could not have been realized without the help of a couple of people.

First of all, I want to express my gratitude to Prof. Yuanhui Zhang for accepting me in his working group and providing me the opportunity to work on such an exciting project. He tried his best to make all materials available that were needed for the work.

Further on, I want to thank Wan-Ting (Grace) Chen, the Microanalysis Lab, the Roy J. Carver Biotechnology Center and the Illinois State Water Survey (B.K. Sharma) for their analytical support.

In addition, I want to thank whole-hearted my colleague and friend Peng Zhang, who spent a lot of time helping me with logistic and experimental issues.

Moreover, I want to warmly thank Nathan Wells for his assistance during the experiments and the interesting discussions.

Last but not least, I want to express my gratitude to the Austrian Marshall Plan Foundation including Angelika Schweighart (TU Vienna), who supported me a lot by providing a scholarship.

Abstract

The aqueous phase after HTL (hydrothermal liquefaction) of wet biomass still contains significant amounts of organic compounds, which is disadvantageous for re-cultivation of microalgae therein and decreases the process efficiency. HTG (hydrothermal gasification) was investigated for its suitability of removing those compounds. A number of catalytic and non-catalytic batch tests were carried out at 350-600 °C and 220-340 bar with a reaction time of 1 h. The aqueous byproduct from HTL of swine manure served as a feed. AC (activated carbon), α-Al_2O_3, TiO_2 (rutile), diatomaceous earth (DE), MnO_2 and Raney-nickel were assessed for their catalytic activity. Raney-nickel and AC showed the highest catalytic activities, whereas Al_2O_3, TiO_2 and DE did not have any catalytic effect. The highest CODr (COD removal efficiency) could be reached at 600 °C and was in the range of 91.3-98.1%. Effective gasification went hand in hand with an increase in pH from 5-6 to about 8-9.

Contents

Acknowledgement 2

Abstract 3

List of Figures 6

List of Tables 8

1. Introduction and theoretical background 9
- 1.1. Motivation . . . 9
- 1.2. Properties of sub- and supercritical water . . . 9
- 1.3. Hydrothermal liquefaction and gasification . . . 10
  - 1.3.1. General aspects . . . 10
  - 1.3.2. Biomass degradation . . . 11
  - 1.3.3. Heterogeneous catalysis in HTG . . . 12
- 1.4. Problem statement . . . 13
- 1.5. Scope of this work . . . 14

2. Experimental setup and analysis 15
- 2.1. Reactor setup . . . 15
- 2.2. Experimental schedule . . . 15
- 2.3. General procedure . . . 16
  - 2.3.1. Preparation of the feed . . . 16
  - 2.3.2. Preparation of the sand bath . . . 17
  - 2.3.3. Preparation of the batch reactor . . . 17
  - 2.3.4. Experimental procedure . . . 18
- 2.4. Analytical tools . . . 18
  - 2.4.1. Separation of the samples . . . 18
  - 2.4.2. COD (Chemical Oxygen Demand) . . . 18
  - 2.4.3. Total nitrogen . . . 19
  - 2.4.4. pH-value . . . 19
  - 2.4.5. TOC (Total Organic Carbon) . . . 19
  - 2.4.6. Water content . . . 19
  - 2.4.7. Inorganic elements . . . 19
  - 2.4.8. GC-MS (Gas Chromatography - Mass Spectrometry) . . . 20
  - 2.4.9. Gas analysis . . . 20

3. Results and discussion 21
- 3.1. Analysis of the feed . . . 21
- 3.2. Water tests . . . 22
- 3.3. Visual observations . . . 22

3.4. First series of tests . . . 23
3.5. Second series of tests . . . 26
3.6. Third series of tests . . . 26
3.7. Fourth series of tests . . . 27
3.8. Fifth series of tests . . . 28

4. Summary and recommendations **30**
4.1. Summary of the experiments . . . 30
4.2. Recommendations for future work . . . 30

A. Batch reactor parts **32**

B. Catalysts **33**

C. GC-MS results **34**

D. Progressions of temperature and pressure **35**
D.1. First series of tests . . . 35
D.2. Second series of tests . . . 41
D.3. Third series of tests . . . 43
D.4. Fourth series of tests . . . 44
D.5. Fifth series of tests . . . 46

E. COD results **48**
E.1. First series of tests . . . 48
E.2. Second series of tests . . . 49
E.3. Third series of tests . . . 49
E.4. Fourth series of tests . . . 49
E.5. Fifth series of tests . . . 50

F. Valve issue **51**

References **52**

List of Figures

1.1. Comparison of the conditions promoting HTL and HTG. 11

2.1. Batch reactor. 15

2.2. Fluidized sand bath. 16

3.1. Relative peak areas of the major organic groups identified in the feed through GC-MS (in %). 21

3.2. Selected examples of liquid/solid reaction products. (a) 450 °C-blank; (b) 500 °C-MnO_2; 600 °C-RaNi; 600 °C-blank (coke residue). 23

3.3. Effect of catalysts on CODr (350 °C; catalyst/feed ratio: 0.1; reaction time: 1 h). . . 24

3.4. Effect of catalysts on CODr (400 °C; catalyst/feed ratio: 0.1; reaction time: 1 h). . . 24

3.5. Effect of catalysts on CODr (450 °C; catalyst/feed ratio: 0.1; reaction time: 1 h). . . 25

3.6. Effect of catalysts on CODr (500 °C; catalyst/feed ratio: 0.1; reaction time: 1 h). . . 25

3.7. Repeat tests for blank, AC and MnO_2 (500 °C; catalyst/feed ratio: 0.1 except for AC_2!!!; reaction time: 1 h). 26

3.8. Effect of a higher catalyst amount on CODr (500 °C; catalyst/feed ratio: 0.2; reaction time: 1 h). 27

3.9. Effect of a RaNi catalyst on CODr (350 °C, 400 °C, 500 °C; catalyst/feed ratio: 0.05; reaction time: 1 h). 28

3.10. Effect of catalysts on CODr at high temperature (600 °C; catalyst/feed ratio: 0.1 for AC and Mn_2, 0.05 for RaNi; reaction time: 1 h). 29

D.1. R1: Blank, R2: AC (350 °C). 35

D.2. R1: Al_2O_3, R2: TiO_2 (350 °C). 35

D.3. R1: DE, R2: MnO_2 (350 °C). 36

D.4. R1: Blank, R2: AC (400 °C). 36

D.5. R1: Al_2O_3, R2: TiO_2 (400 °C). 37

D.6. R1: DE, R2: MnO_2 (400 °C). 37

D.7. R1: Blank, R2: AC (450 °C). 38

D.8. R1: Al_2O_3, R2: TiO_2 (450 °C). 38

D.9. R1: DE, R2: MnO_2 (450 °C). 39

D.10. R1: Blank, R2: AC (500 °C). 39

D.11.R1: Al_2O_3, R2: TiO_2 (500 °C). 40
D.12.R1: DE, R2: MnO_2 (500 °C). 40
D.13.R1: Blank_1, R2: Blank_2 (500 °C). 41
D.14.R1: AC_1, R2: AC_2 (500 °C). 41
D.15.R1: MnO_2_1, R2: MnO_2_2 (500 °C). 42
D.16.R1: AC_3, R2: AC_4 (500 °C). 43
D.17.R1: MnO_2_3, R2: MnO_2_4 (500 °C). 43
D.18.R1: RaNi, R2: RaNi_1 (350 °C). 44
D.19.R1: RaNi, R2: RaNi_1 (400 °C). 44
D.20.R1: RaNi, R2: RaNi_1 (500 °C). 45
D.21.R1: Blank, R2: Blank_1 (600 °C). 46
D.22.R1: RaNi, R2: RaNi_1 (600 °C). 46
D.23.R1: AC, R2: AC_1 (600 °C). 47
D.24.R1: MnO_2, R2: MnO_2_1 (600 °C). 47

List of Tables

3.1. Feedstock characteristics. 21
3.2. Amount of feed used depending on the reaction temperature. 22
A.1. Swagelok parts of the batch reactors. 32
B.1. Catalysts used for the experiments. 33
C.1. Results gained from GC-MS analysis of the feed. 34
E.1. COD data of the first series of tests. 48
E.2. COD data of the second series of tests. 49
E.3. COD data of the third series of tests. 49
E.4. COD data of the fourth series of tests. 49
E.5. COD data of the fifth series of tests. 50

1. Introduction and theoretical background

1.1. Motivation

In 2012 the global primary energy supply reached 13 371 Mtoe, of which only 10.0% were provided through biofuels and waste and only 2.4% through hydropower [1]. As a consequence, the atmospheric carbon dioxide concentration has been rising and reached nearly 400 ppm in 2014 (compared to 317 ppm in 1960) [2]. The IPCC (Intergovernmental Panel on Climate Change) has been working for years collecting and evaluating environmental data, which have proved that anthropogenic emissions of greenhouse gases influence the climate system. In addition, the IPCC reports demonstrate how the world would look like in 100 years if human kind did not change the way of living [3]. More intense research in the fields of renewable energy and development of more sustainable technologies are urgently needed to stop this transformation and to meet the energy demand at the same time.

In the last few decades the interest in gaining energy from biomass has increased. However, many biomass sources contain high amounts of water, which is undesirable for classical liquefaction- and gasification processes. As a result, so-called *hydrothermal processes* have been developed, which comprise thermochemical conversion technologies in hot compressed water [4]. In the following sections the chemistry in sub- and supercritical water will be summarized and the potential and the challenges of the hydrothermal technologies outlined.

1.2. Properties of sub- and supercritical water

Water is non-toxic, has no negative impact on the environment and can be found in high amounts in most plants and living creatures. In biomass conversion processes water plays an important role as a solvent, a reactant, a catalyst and as a catalyst precursor [5, 6]. The reasons are related to the properties of (pure) water above and below its critical point:

- Phase regions:

  At the critical point of water (T_c = 374 °C, p_c = 22.1 MPa, ρ_c = 322 kg/m^3) the density of the liquid- and the vapor phase reach the same value and the two phases combine to a single homogenous fluid [7]. Water at $T > T_c$ and $p > p_c$ is called *supercritical water*, otherwise *subcritical water*.

- Density and viscosity:

  Compared to liquid water, supercritical water has a lower viscosity resulting in a higher mass transfer rate. Compared to water vapor, supercritical water has a higher density resulting in a higher heat transfer rate [5, 7].

- Relative permittivity:

  The static (zero-frequency limit) relative permittivity is a dimensionless parameter that describes the polarity of a solvent compared to vacuum and the strength of its electrostatic interactions with ionic solutes [8, 9]. If a solvent has a high static relative permittivity, it is very polar and has a high solubility for dissociating ionic salts. If a solvent has a low static relative permittivity, it is non-polar and has a high solubility for non-polar organics and gases [10]. The static relative permittivity of liquid water decreases drastically with increasing temperature, especially when reaching the supercritical region. At 30 MPa water has a static relative permittivity of about 80 at 25 °C and less than 2 at 450 °C [9]. In comparison, at ambient conditions methanol has a static relative permittivity of about 33, acetone of about 21 and diethylether of about 4 [11].

- Ionization constant:

  At pressures between 0.1 MPa and 50 MPa the ionization constant of water, which is defined as the product of its ion concentrations resulting from self-dissociation, increases with increasing temperature from about 10^{-14} (mol^2L^{-2}) at room temperature to about 10^{-11} (mol^2L^{-2}) at 250-300 °C. After reaching a maximum it decreases drastically again [12]. In the temperature range of 250-300 °C, where the ionization constant is around three orders of magnitude higher than at room temperature , water does not only act as a solvent but also as a catalyst for ionic reactions like acid- and base catalyzed reactions [13].

1.3. Hydrothermal liquefaction and gasification

1.3.1. General aspects

Hydrothermal processes cover biomass conversion technologies in a water-rich milieu at elevated temperatures and sufficient pressures to keep the water in either liquid or supercritical state [14]. Depending on the temperature, hydrothermal processing is divided into three regions. At temperatures below about 250 °C it is known as *hydrothermal carbonization* and the main product is hydrochar, which is similar to low rank coal. At temperatures between around 250 and 350 °C it is known as *hydrothermal liquefaction* (HTL) and the main product is bio-crude, which is similar to petroleum crude. At temperatures higher than about 350 °C the process is known as *hydrothermal gasification* (HTG) and the main product is a synthetic fuel gas [15]. Moreover, Osada *et al.* [16] defined three regions for hydrothermal gasification: subcritical water gasification (< 374 °C), low-temperature supercritical water gasification (374-500 °C) and high-temperature supercritical water gasification (> 500 °C). However, the boundaries of those regions are not strict. For example, Faeth *et al.* [17] were able to produce high yields of bio-crude through *fast* HTL of the microalgae Nannochloropsis sp. at 600 °C and at a very short reaction time of 1 min (The reaction time was not long enough for gasification.).

Nearly all kinds of biological/organic materials could be processed hydrothermally. To avoid competition with the food industry, much research and development is focusing on using residuals, wastes and low intensity energy crops like crop residues, wood (residues), food processing waste, manure, sewage sludge, switchgrass and algae (macro-, microalgae). A suitable dry matter content of the feed for hydrothermal treatment is in the range of 5-35 wt%. Feedstocks with high water content (e.g. algae) can be blended with feedstocks that have a low water content (lignocellulosic biomass) to get an appropriate dry matter content [5,14,15,18].

In the next few sections the important processes and coherences related to HTL and HTG will be described.

1.3.2. Biomass degradation

In sub- and supercritical water at temperatures higher than about 250 °C the polymeric structure of biomass is broken down to smaller molecules. Depending on temperature, reaction time and presence of catalysts, the reaction products are mainly liquid or gaseous components (see Figure 1.1).

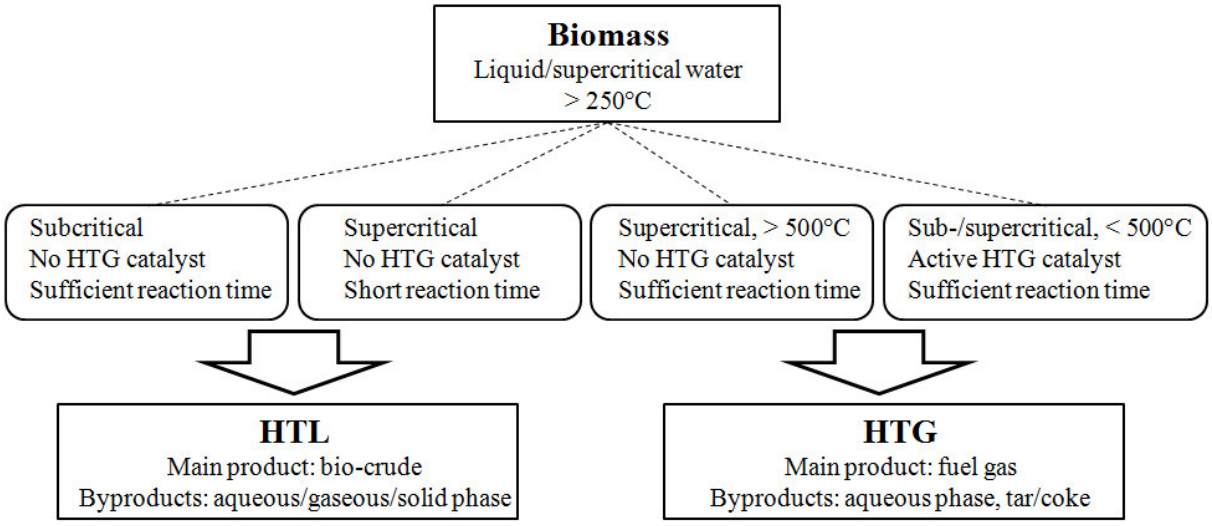

Figure 1.1: Comparison of the conditions promoting HTL and HTG.

In the absence of an active gasification catalyst, HTL is the dominant conversion process either under subcritical conditions if the reaction time is long enough for biomass degradation to liquid products [19] or under supercritical conditions if the reaction time is not long enough for further degradation to gaseous products [17]. The reactions that take place during HTL are very complex and their exact pathways and kinetics are difficult to determine due to the big variety of biological materials. The attempts of understanding those mechanisms have been summarized in a few comprehensive reviews [4, 14, 20, 21]. The HTL product consists of a bio-crude phase, an aqueous phase, a gas phase and a solid residue phase [22]. The bio-crude is a very viscous oil that has a high oxygen content of up to about 20 wt% [14]. It is a complex

mixture containing various hydrocarbons, acids, alcohols, ethers, amides, ketones, phenols, benzofurans, N-heterocyclic compounds. The same components found in the bio-crude can be detected in low concentrations in the aqueous phase due to their slight solubility in water. The major groups appearing there are acids and N-heterocyclic compounds [19, 23]. The gas produced by HTL mainly consists of CO_2 [24, 25].

At temperatures above 500 °C (high-temperature supercritical region) and sufficient reaction time, HTG is the dominant conversion process. Below 500 °C (subcritical-, low-temperature supercritical region) complete biomass degradation is only possible in the presence of an active gasification catalyst [14,19]. The main gasification reactions can be summarized by the following equations [26, 27]:

$$CH_xO_y + (2-y)H_2O \leftrightarrow CO_2 + (2-y+x/2)H_2 \quad ... \quad \triangle H_R^\circ > 0 \tag{1.1}$$

$$CH_xO_y + (1-y)H_2O \leftrightarrow CO + (1-y+x/2)H_2 \quad ... \quad \triangle H_R^\circ > 0 \tag{1.2}$$

$$CO + H_2O \leftrightarrow CO_2 + H_2 \quad ... \quad \triangle H_R^\circ = -41\,\text{kJ/mol} \tag{1.3}$$

$$CO + 3H_2 \leftrightarrow CH_4 + H_2O \quad ... \quad \triangle H_R^\circ = -211\,\text{kJ/mol} \tag{1.4}$$

$$CO_2 + 4H_2 \leftrightarrow CH_4 + 2H_2O \quad ... \quad \triangle H_R^\circ = -233\,\text{kJ/mol} \tag{1.5}$$

Equations 1.1 and 1.2 represent the steam reforming reactions, Equation 1.3 is the water-gas shift reaction and Equations 1.4 and 1.5 express the methanation reactions. Furthermore, Equations 1.3, 1.4 and 1.5 describe the equilibrium between CO, CO_2, H_2, CH_4 and H_2O. In addition, traces of hydrocarbons, like C_2H_6 and C_2H_4, might be produced, too [28]. According to Le Chatelier's principle, the following conclusions can be drawn: Since Equations 1.3, 1.4 and 1.5 are exothermic and the number of moles decreases during the methanation reactions, lower temperatures and higher pressures favor the formation of CH_4, whereas higher temperatures and lower pressures favor the formation of H_2. A number of experimental and thermodynamic studies confirmed a higher CH_4 concentration at lower temperatures and a higher H_2 concentration at higher temperatures. Interestingly, they showed that pressure had no significant influence on the gasification results [14, 28]. Tar and coke are undesired byproducts, which are relatively unreactive compounds. Although their formation is suppressed by the solvent properties of near- and supercritical water (see Section 1.2), they might be formed in the absence of an active gasification catalyst or during heat-up [5, 14].

1.3.3. Heterogeneous catalysis in HTG

Under subcritical and low-temperature supercritical conditions (350-500 °C) an active catalyst is needed to achieve high gasification efficiencies [16]. The two methanation reactions (Equations 1.4 and 1.5) exhibit high activation energies without a catalyst and obtain low reaction rates resulting in a product composition far from the thermodynamic equilibrium [5]. Compared to

homogeneous catalysts, heterogeneous catalysts are usually more selective, easier recyclable and environmentally friendlier [29]. The findings regarding heterogeneous catalysis in HTG have been summarized in a couple of excellent reviews [5,27–35]. Many different materials have been tested for their suitability as an HTG catalyst. They can be divided into three categories: activated carbon, (un)supported transition metals, metal oxides [31].

Activated carbon showed high catalytic activity at relatively high temperatures (around 600 °C), but deactivation occurred after about 4 h in a continuous test [36]. Raney-nickel is an example for an unsupported metal catalyst that has gained a lot attention due to its high activity [31]. However, its skeletal structure is not stable in the hydrothermal environment and undergoes sintering [37]. In addition, oxidation seems to be a major cause for deactivation [38]. A number of materials have been tested for their suitability as catalyst supports. Only a few showed sufficient stability in sub- and supercritical water, including carbon (activated, graphitic, pyrolytic, nanotubes), ZrO_2 (monoclinic), TiO_2 (rutile) and α-Al_2O_3 [5,31]. The two most frequently investigated supported metal catalysts are Ni and Ru. They show very high activities on different supports over a wide temperature range [31]. Nevertheless, they both have considerable drawbacks. Ni might deactivate through sintering or oxidation [5,33] and Ru is prone to poisoning by sulfur [32], which can be found in all biomass types in organic and inorganic forms due to its biogeochemical cycle [39]. Although metal oxides have been rather used as a catalyst support for hydrothermal gasification, a few of them have been tested for their catalytic activity including CaO, ZrO_2, CeO_2, Fe_2O_3, RuO_2 and MnO_2 [28,31,33].

Apart from controlled catalysis through the addition of certain catalysts, uncontrolled catalysis can take place in two ways. Firstly, alkali salts, which are present in various biomass sources [40], have a catalytic effect on different degradation reactions [4]. Secondly, most of the reactors used for hydrothermal conversion of biomass are made of alloys (e.g. Inconel, Hastelloy) containing high amounts of Ni, which can act as a catalyst at the surface of the inner wall [14,29].

1.4. Problem statement

At the University of Illinois at Urbana-Champaign (UIUC) an integrated waste-to-energy system, called *Environment-Enhancing Energy* (E^2-Energy), was developed [41]. The idea is to combine algal wastewater treatment with bio-fuel production via HTL. In this process the CO_2-rich gaseous phase and the aqueous phase from the HTL step are recycled for algae cultivation. Moreover, important nutrients for algae growth like N, P and K, which can be found in high amounts in the aqueous phase, are recycled, too [42–45].

Recent studies have tested the suitability of the aqueous HTL byproduct for algae cultivation. It turned out that some components therein had an inhibiting effect on the algae growth. The process water had to be significantly diluted (> 100 times) to gain acceptable growth rates. Especially autotrophic microbes seem to be very sensitive to the organic substrate level [41,43,46]. A promising way to remove the organic compounds in the aqueous HTL byproduct

is through HTG [15]. Elliott and co-workers effectively demonstrated cleanup and fuel gas production from water soluble organics through catalytic HTG. They were able to achieve high carbon gasification efficiencies when continuously processing algal HTL wastewater over a 7.8%-Ru/C catalyst at around 350 °C and 20 MPa [47,48].

To the best of our knowledge, the studies of Elliott's group [47,48] are the only ones published so far describing HTG of aqueous HTL byproduct. Further investigations at different temperatures and with the use of various catalysts are of great interest to evaluate the applicability of a combined HTL-HTG process in more detail.

1.5. Scope of this work

HTG experiments should be performed in a batch mode. The aqueous byproduct from HTL of swine manure, which had been produced during a continuous test in summer 2014, should be used as a feed. The influence of temperature and catalyst on the gasification efficiency (expressed as COD removal efficiency) should be assessed. Activated carbon (AC), α-Al_2O_3, TiO_2 (rutile), diatomaceous earth (DE) and MnO_2 should be examined for their catalytic suitability due to following reasons:

- Since Ru/C was the only catalyst used so far for HTG of HTL wastewater, it was decided to investigate "simple", low-cost materials first before testing "fancy", high-cost materials including noble metals.
- Only a few metal oxides have been tried as HTG catalysts, although some of them showed catalytic activity [28,31].
- α-Al_2O_3 and rutile TiO_2 seem to be stable in a hydrothermal environment [5,49].
- MnO_2 should be stable in a hydrothermal environment up to about 500 °C [5,49] and showed catalytic activity when gasifying black liquor at 500 °C [28].
- Only a few studies have been published describing the use of AC as a HTG catalyst [36,50,51].
- DE was included in the catalyst screening because it was available due to experiments of other group members.

In addition, comparison tests with Raney-nickel (RaNi), which is a well-known active HTG catalyst [31], should be carried out. Nevertheless, the main purpose of this project was to develop an experimental setup and procedure for HTG tests and to conduct pioneering experiments.

2. Experimental setup and analysis

2.1. Reactor setup

A reactor setup similar to the ones used by Prof. Vogel's [52] and Prof. Savage's group [53] was designed. The batch reactors (Figure 2.1) consisted of a stainless steel tube (length: 14 in, outer diameter: 0.5 in, wall thickness: 0.083 in), a stainless steel capillary (length: 10 in, outer diameter: 0.125 in, wall thickness: 0.035 in), a pressure gauge, a high-pressure valve and corresponding fittings. All parts were purchased from Swagelok and selected to meet pressure- and temperature ratings (see Appendix A).

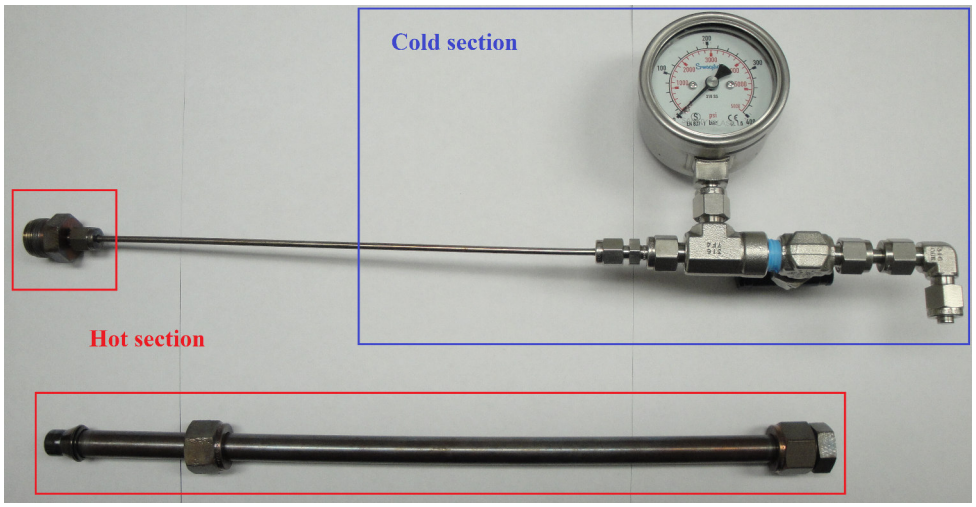

Figure 2.1: Batch reactor.

A fluidized sand bath (Techne, SBL-2D) was used as a heater including a controller (Techne, TC-8D), which regulated the temperature at the bottom of the sand bath. An additional thermocouple was dipped into the sand bath from the top ensuring uniform temperature distribution and sufficiently turbulent fluidization. The vessel of the sand bath was covered with a shield, which was made of stainless steel wires wrapped in aluminum foil, to prevent spilling over of sand. A simple construction was used for mounting the batch reactors (see Figure 2.2).

2.2. Experimental schedule

Based on the scope of this work (see Section 1.5) and the experience gained during the experiments, the assessment was conducted by an experimental approach including the following steps:

1. A catalyst screening of AC, α-Al_2O_3, TiO_2 (rutile), DE and MnO_2 in the temperature range of 350-500 °C was performed with the aim to identify the promising catalysts.
2. The most interesting tests of step 1 were repeated for consistency reasons.

3. The catalytic experiments of step 2 were conducted with a higher catalyst/feed ratio to determine the influence of the catalyst amount.
4. Comparison tests using a RaNi catalyst were performed.
5. Additional high-temperature experiments at 600 °C were conducted.

Figure 2.2: Fluidized sand bath.

2.3. General procedure

2.3.1. Preparation of the feed

The starting material was an aqueous product, which had been produced by Mitchell James Minarick during a continuous HTL test of swine manure in summer 2014 and had been stored in a cold room at 5 °C. About 2 L of the wastewater were filtered twice (Whatman®, grade 1) to make use of depth- and surface (cake) filtration, stored in a glass jar and steadily kept in a refrigerator at 5 °C, unless the feed was needed for a test or analysis.

2.3.2. Preparation of the sand bath

In the morning of an experimental day the oil level and the oil filter of the air compressor were checked and – if necessary – refilled and cleaned. Then the air compressor and the heaters of the sand bath were turned on and the setpoint of the temperature controller defined. Since the thermocouple of the controller was positioned at the bottom of the sand bath, where the temperature was a few degrees lower than at the top, the setpoint was usually defined at 5-10 °C above the desired temperature. During heat-up, which took about 2-3 h, the fluidization was monitored and the air flow adjusted if needed. A small temperature difference between top and bottom of the sand bath at steady-state indicated adequate fluidization.

2.3.3. Preparation of the batch reactor

Before a reactor could be used for a new experiment, it had to be cleaned. The Swagelok fittings of the hot section (see Figure 2.1) were brushed under tap water, sonicated (Kendal, HB-S-49DHT), rinsed with DI (deionized) water and dried with pressurized air. The internal wall of the reaction volume (tube, cap, reducer) was brushed under tap water with soap, rinsed with ethanol and finally rinsed with DI water. The cold section (capillary, T-piece, valve), which was moist inside from a previous test, was dried and rinsed with Helium.

Assembling, filling and pressurization of the reactor was done in the following way:

1. The threads of the reactor cap were lubricated with a nickel paste (LOCTITE® N-5000™) to protect the threads from the sand of the bath and to ease opening later on.
2. The cap was attached to the tube and the connection tightened.
3. When a blank test (no catalyst) was conducted, the entire feed was added to the reaction tube with the help of a pipette. When a catalytic test was conducted, half of the feed was added first, then the catalyst funneled and the other half of the feed added finally. All catalysts (Appendix B) were used as they had been delivered. Information regarding the amount of feed will be discussed in Section 3.2.
4. The threads of the reducer, which connected the reactor tubing and the capillary, were lubricated with a nickel paste for the same reasons as described before.
5. The reducer (including the cold section) was attached to the tube and the connection tightened.
6. The reaction volume was rinsed three times by pressurizing (to about 60 bar) and depressurizing the system three times with Helium. To avoid water evaporation during later heat-up, the reactor was kept at 40 bar after the third flushing.
7. The reactor was inspected for leakage with the help of soap water. Comments regarding leakages can be found in Section 3.2.

2.3.4. Experimental procedure

As soon as the sand bath had reached steady-state with respect to temperature, the tests could be started. Usually two reactions were carried out simultaneously. The fittings of the reaction tubes were treated with pressurized air to remove residual soap water (from the leakage test) and nickel lubricant. Moreover, the reactors were shaken gently to mix feed and catalyst. Then the reactors were dipped into the sand bath and mounted and a stopwatch was started. The temperatures at the bottom and the top of the sand bath as well as the pressures inside the reactors were read off and noted down every minute for the first ten minutes, afterwards every five minutes. The progressions of temperature and pressure of all reactions can be found in Appendix D. After 1 h the reactors were taken out, quenched in a bucket filled with tap water and cooled down to room temperature.

As a next step, the product gases were released and did not have to be collected because no instrument for appropriate gas analysis was available (see Section 2.4.9). Finally, the reactors were opened at the top of the reaction tube, the liquid/solid products poured into 15 mL plastic vials and the samples stored in a refrigerator/cold room at 5 °C.

2.4. Analytical tools

2.4.1. Separation of the samples

The reaction products contained a liquid and a solid (tar, coke, catalyst) phase and had to be separated for COD analysis. The samples were taken out of the refrigerator/cold room and homogenized (Barnstead/Thermolyne®, Maxi Mix II, Type 37600) for a few seconds. Afterwards they were centrifuged (International Equipment Company, IEC Centra-7 Centrifuge) at 5000 rpm for 15 min. As a result, the liquid phases floated on the top and could be pipetted into new 15 mL plastic vials. The samples were kept in a refrigerator/cold room at 5 °C.

2.4.2. COD (Chemical Oxygen Demand)

The COD of the feed and the liquid samples had to be measured to calculate the CODr (COD removal efficiency):

$$CODr = \left(1 - \frac{COD\ of\ aqueous\ residue}{COD\ of\ feed}\right) * 100\% \tag{2.6}$$

Before the samples could be analyzed, they had to be diluted 100-times to stay below the allowed concentration maximum. Digestion and measurement were carried out according to Hach® Method 8000 using a COD reactor (Hach®, Product#: 2125915) and a DR/2000 Spectrophotometer (Hach®, Product#: 4480000, Method#: 435). Whenever a new measurement

series was carried out, correct calibration of the analyzer was checked by measuring a standard solution (Hach®, Product#: 1218629). Each diluted sample was analyzed 3-times to provide the SD (Standard Deviation) of the measurements.

2.4.3. Total nitrogen

The total nitrogen content of the feed was determined. Before the feed sample could be analyzed, it had to be diluted 100-times to stay below the allowed concentration maximum. Digestion and measurement were carried out according to Hach® Method 10072 using a COD reactor (Hach®, Product#: 2125915) and a DR/2010 Spectrophotometer (Hach®, Product#: 4930000, Method#: 395). Correct calibration of the analyzer was checked by measuring a standard solution (Hach®, Product#: 194749). The diluted feed sample was analyzed 3-times to provide the SD of the measurements.

2.4.4. pH-value

The pH-values of the feed and some products were determined using pH paper (Micro Essential Laboratory, Hydrion®).

2.4.5. TOC (Total Organic Carbon)

The TOC of the feed was analyzed according to SM 5310B by Illinois State Water Survey. NVOC (Non-Volatile Organic Carbon) was measured using a Tekmar Dohrmann Apollo 9000 HS carbon analyzer, a Gilson 223 sample changer and a TOC Talk software. 500 µL of a 2000-times diluted sample were injected into the instrument and combusted catalytically (platinum) at 850 °C. The CO_2 formed was measured directly by a NDIR (Non-Dispersive InfraRed) sensor.

2.4.6. Water content

The water content of the feed was determined according to ASTM D6304 by Illinois State Water Survey. The measurements were repeated until the SD was acceptably low.

2.4.7. Inorganic elements

The feed was also analyzed for inorganic elements by the Mycroanalysis Laboratory. Ca, K, Mg, Na, P and S were measured via ICP-OES (PerkinElmer 2000DV), whereas Cl with an ion selective electrode (Thermo Scientific™ Orion™) [54].

2.4.8. GC-MS (Gas Chromatography - Mass Spectrometry)

To get additional information about the chemical composition of the feed, GC-MS analysis was conducted by Wan-Ting (Grace) Chen with the help of the Roy J. Carver Biotechnology Center. A description of the analytical procedure can be found elsewhere [23].

2.4.9. Gas analysis

With the use of a gas chromatograph equipped with a TCD (Thermal Conductivity Detector), helium is an appropriate carrier gas for analysis of CO, CO_2, CH_4, C_2H_6 and C_3H_8 because of the big difference in thermal conductivity. However, helium is not appropriate for analysis of hydrogen due to the rather small difference in thermal conductivity [37, 55]. Unfortunately, all gas chromatographs found on campus used helium as the carrier gas and were not able to analyze gas samples containing H_2, CO, CO_2 and CH_4, which were diluted by helium or nitrogen (because of pressurization, see Section 2.3.3). Furthermore, no instrument was available that could be set up for such kind of gas mixtures.

3. Results and discussion

3.1. Analysis of the feed

For evaluation of the experiments and comparison of the results with literature, it was very important to get information regarding the composition of the feed. The analytical results are summarized in Table 3.1 and in Figure 3.1.

Table 3.1: Feedstock characteristics.

Parameter	Unit	Value	SD
Water content	wt%	93	2.4
COD	mg/L	96520	973.1
TOC	mg/L	33400	-
Total nitrogen	mg/L	7367	152.8
Ca-content	mg/L	31	0
K-content	mg/L	4131	25
Mg-content	mg/L	222	1
Na-content	mg/L	902	7
P-content	mg/L	69	0
S-content	mg/L	331	5
Cl-content	mg/L	3700	-
pH value	-log(mol/L)	5-6	-

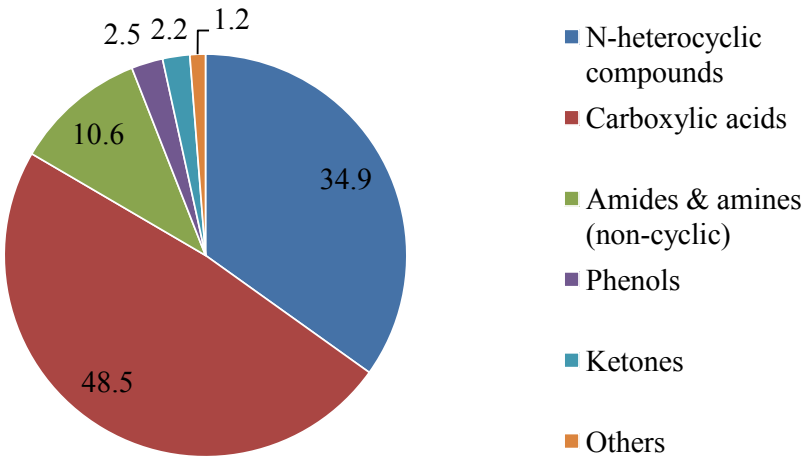

Figure 3.1: Relative peak areas of the major organic groups identified in the feed through GC-MS (in %).

The concentrations of COD and TOC are in a typical range for post-HTL wastewater [41].

The total nitrogen content is similar to one gained after HTL of swine manure with a dry matter content of 20 wt% at around 300 °C [44]. High concentrations of K, Na and Cl were measured, too, after HTL of the microalgae Spirulina [43]. Surprisingly, our P-content is much lower compared to the one measured in earlier studies [41, 44]. As already determined previously [41], the aqueous byproduct from HTL of swine manure is more acidic (pH 5-6) than the aqueous byproduct from algal HTL (pH 7-8) [41, 43, 47, 48]. The GC-MS results, showing mostly carboxylic acids and N-heterocyclic, are in accordance with literature [23, 46]. More detailed GC-MS results can be found in Appenix C.

3.2. Water tests

Before the actual tests with the real feed were started, water tests were carried out, firstly, to get familiar with handling of the experimental procedure and, secondly, to determine the amount of feed needed to get into the desired pressure range of 220-340 bar at a certain reaction temperature. The minimum pressure was defined by the critical pressure of water, whereas the maximum pressure was limited by the pressure ratings of the Swagelok parts. Although this is a wide pressure range, the pressure inside the batch reactors turned out to be very sensitive with respect to feed volume and temperature, especially in the area of the liquid-supercritical phase change. At the beginning of the tests, the thermodynamic data of water [7] helped to estimate the correct feed amount. However, it took a couple of tests to obtain the relations summarized in Table 3.2. Leakage issues, which frequently occurred during those water tests, made the determinations even more difficult. In most of the cases, leakages arose at the 0.5 in nut& ferrule connections of the reaction tube. After taking more care of cleaning, lubricating the threads with a nickel paste (see Section 2.3.3) and tightening the connections more than suggested by Swagelok [56], the leakage issues became much better. Finally, it was even possible to conduct all experiments with only two reactors.

Table 3.2: Amount of feed used depending on the reaction temperature.

Reaction temperature (in °C)	Feed amount (in mL)
350	16.0
400	10.0
450	6.0
500	3.5
600	1.8

3.3. Visual observations

Although visual observations cannot give quantitative information, they deliver valuable qualitative information. They might reduce the number of experiments and analytical costs and

are helpful for prospective workers with interpretation of their first results. Figure 3.2 shows selected examples of the liquid/solid reaction product. The darker the liquid phase was, the lower was the gasification efficiency (Figure 3.2a). In such a case a tarry phase was produced, which indicated that HTL had taken place rather than HTG. This was the case when the temperature was too low or when the catalyst was not active enough (see Section 1.3). The color of the liquid product became clearer with increasing temperature and catalytic activity showing better gasification (Figure 3.2b,c). Despite the high gasification efficiencies at high temperatures, some coke was produced, too (Figure 3.2d).

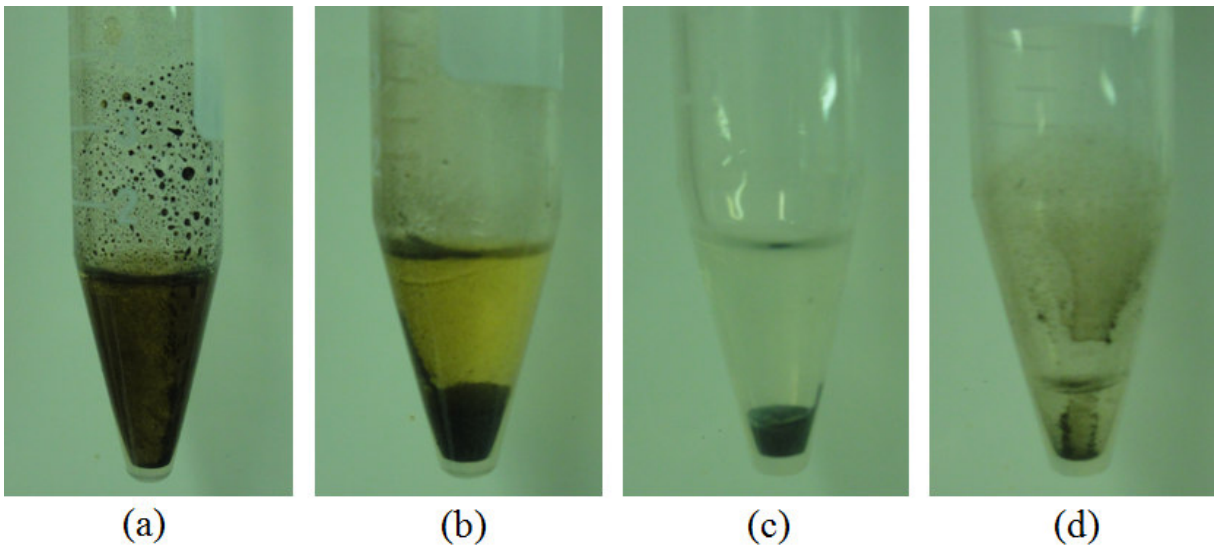

Figure 3.2: Selected examples of liquid/solid reaction products. (a) 450 °C-blank; (b) 500 °C-MnO_2; 600 °C-RaNi; 600 °C-blank (coke residue).

3.4. First series of tests

As a first step, a temperature/catalyst screening was conducted. Reactions at 350, 400, 450 and 500 °C with and without the addition of heterogeneous catalysts (AC, Al_2O_3, TiO_2, DE, MnO_2) were carried out. The reaction time was 1 h to make sure that equilibrium was reached. In all catalytic tests, the catalyst/feed ratio (in $g_{Catalyst}/g_{Feed}$) was 0.1. The aim was to find out which temperature range and catalysts were worthy of being considered in the following experiments. Therefore, each experiment was performed only once. The dependence of the CODr on temperature and catalyst is depicted in Figures 3.3, 3.4, 3.5 and 3.6.

As expected from literature reviews (see Section 1.3), the CODr increased with temperature. Only AC and MnO_2 showed considerable catalytic activity. The CODr of the tests with Al_2O_3 was only slightly higher at 350, 400 and 450 °C than the ones of the blank tests. In comparison, Waldner [37] reached a carbon conversion of 26.9% when continuously gasifying a 10 wt% synthetic liquified food solution over α-Al_2O_3 with a WHSV (weight hourly space velocity) of 27.2 h^{-1} at 400 °C and 300 bar. TiO_2 showed slight catalytic activity only at 400 °C. At higher

temperatures the CODr was even lower than the ones of the blank tests. An inhibition effect of TiO_2 on the gasification efficiency was also observed by Youssef when gasifying an aqueous solution containing 9000 mg/L starch and 18 000 mg/L catechol at 500 °C and 280 bar [57]. DE did not show any catalytic activity and seemed to rather have an inhibitory influence, too.

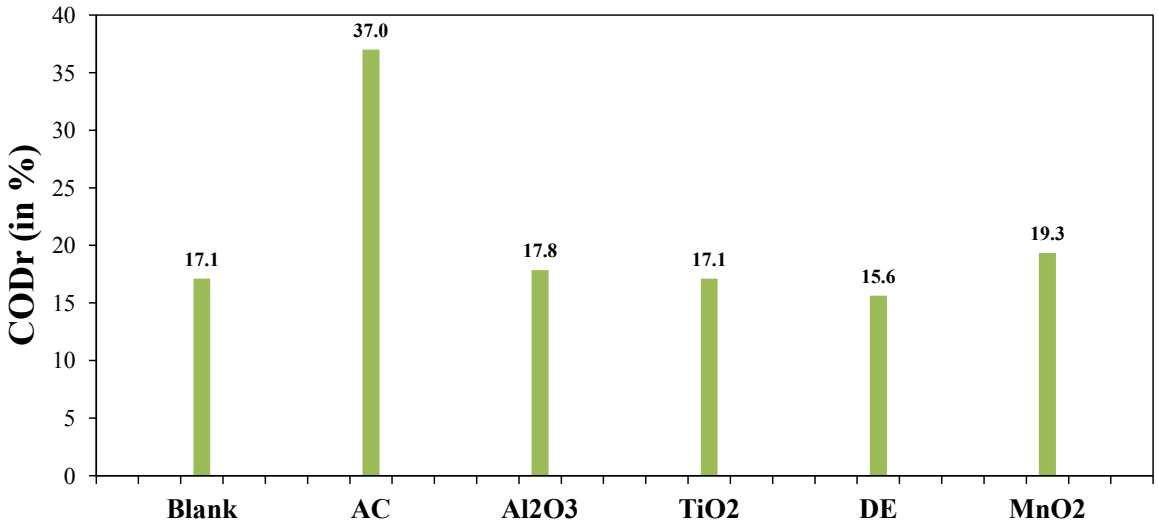

Figure 3.3: Effect of catalysts on CODr (350 °C; catalyst/feed ratio: 0.1; reaction time: 1 h).

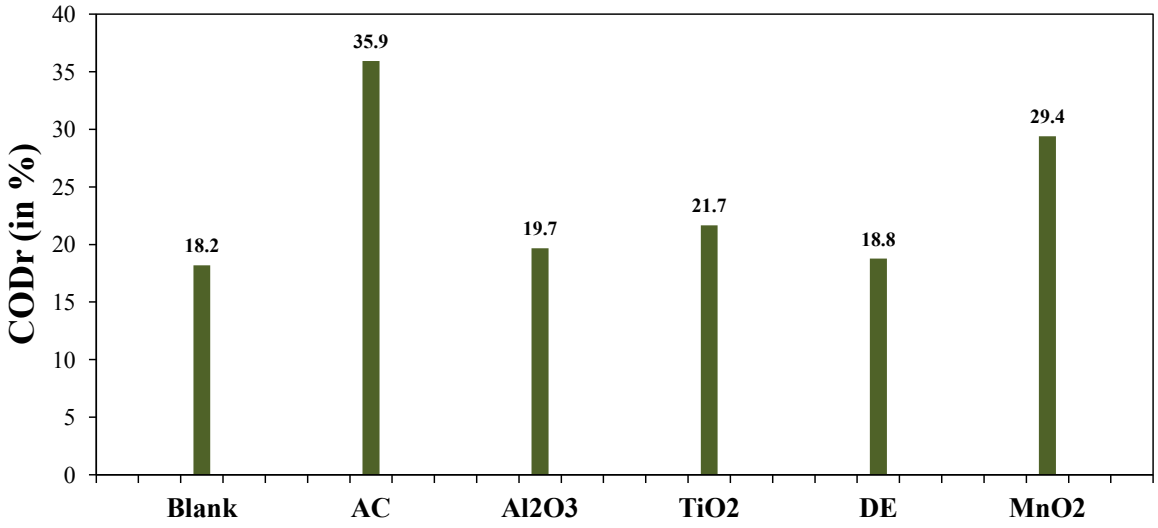

Figure 3.4: Effect of catalysts on CODr (400 °C; catalyst/feed ratio: 0.1; reaction time: 1 h).

AC showed the highest catalytic activity and resulted in the highest CODr at each temperature. The results from the tests at 350 and 400 °C with AC suggest that a phase change from sub- to supercritical state did not have a significant influence on the gasification results in terms of CODr. Sato *et al.* [58] stated a carbon gasification efficiency of 12.6% after HTG of bean curd refuse for 30 min over AC at 400 °C (1 g_{AC}/g_{Refuse}). Yamagouchi *et al.* [59] reached a carbon gasification efficiency of 8.4% when gasifying a 3.2 wt% lignin solution for 1 h at 400 °C and

370 bar with charcoal (1.5 $g_{Charcoal}/g_{Lignin}$). Xu *et al.* [36] were able to reach a carbon gasification efficiency of 51% through continuous HTG of a 1 M glucose solution over AC with a WHSV of 13.5 h^{-1} at 500 °C and 345 bar. Youssef *et al.* [60] reached a CODr of 66% when gasifying hog manure for 30 min over AC (2.5 g_{AC}/mL_{Manure}) at 500 °C and 280 bar.

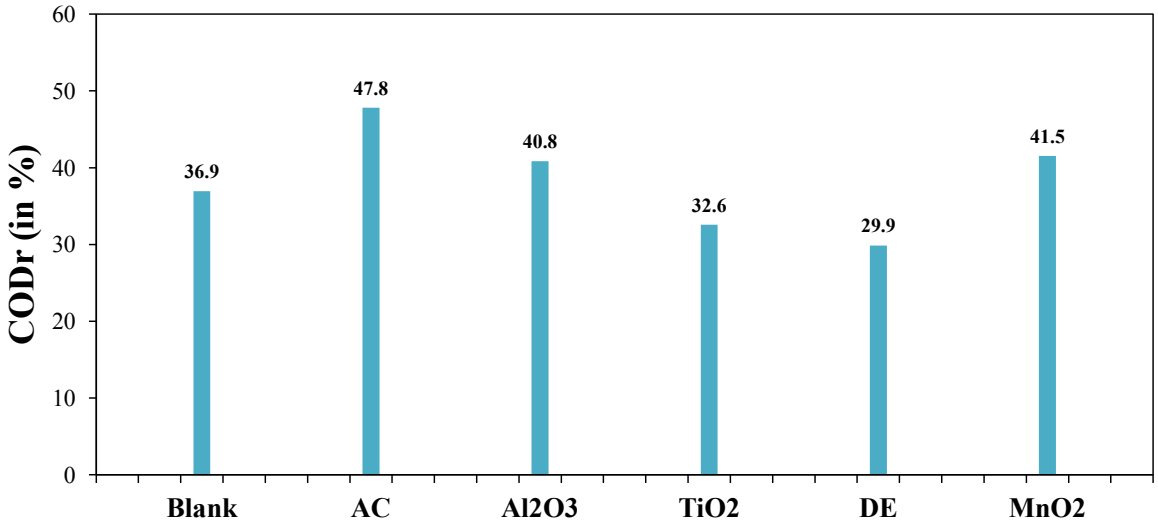

Figure 3.5: Effect of catalysts on CODr (450 °C; catalyst/feed ratio: 0.1; reaction time: 1 h).

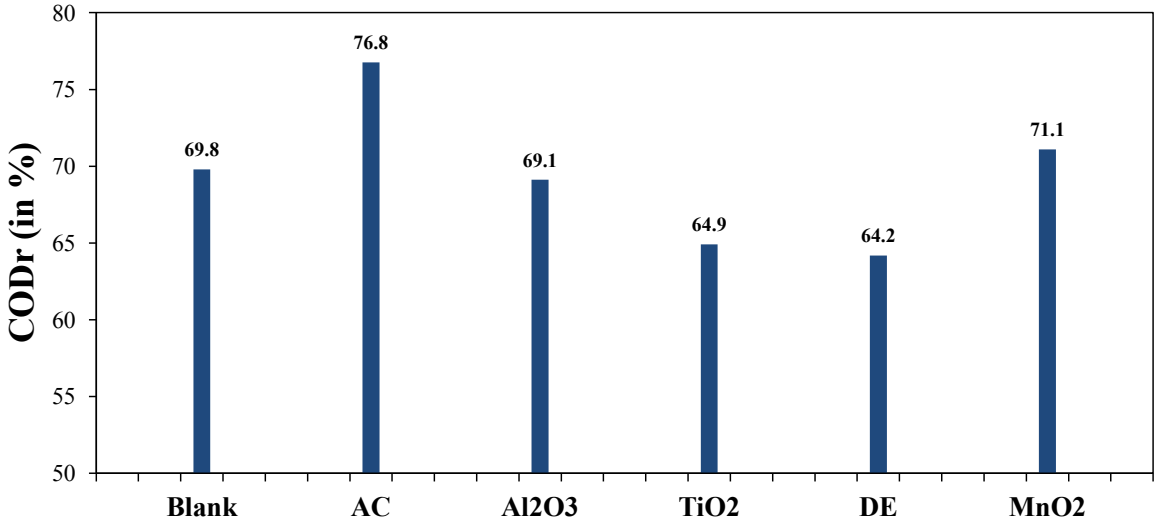

Figure 3.6: Effect of catalysts on CODr (500 °C; catalyst/feed ratio: 0.1; reaction time: 1 h).

The second most active catalyst turned out to be MnO_2. Its activity compared to the blank tests was the highest at 400 and 450 °C. In comparison, Guo [28] reported a CODr of 96.7% when he gasified a 7.8 wt% black liquor solution for 10 min over MnO_2 (0.1 g_{MnO_2}/g_{Liquor}) at 500 °C.

3.5. Second series of tests

In the first test series, only AC and MnO_2 showed some catalytic activity and the CODr reached high values only at 500 °C. Those tests were identified as promising systems for further examination. To have more reproducible results, the blank tests and the catalytic tests with AC and MnO_2 at 500 °C were repeated each twice. Like before, the reaction time was 1 h and the catalyst/feed ratio 0.1. The results regarding CODr are showed in Figure 3.7.

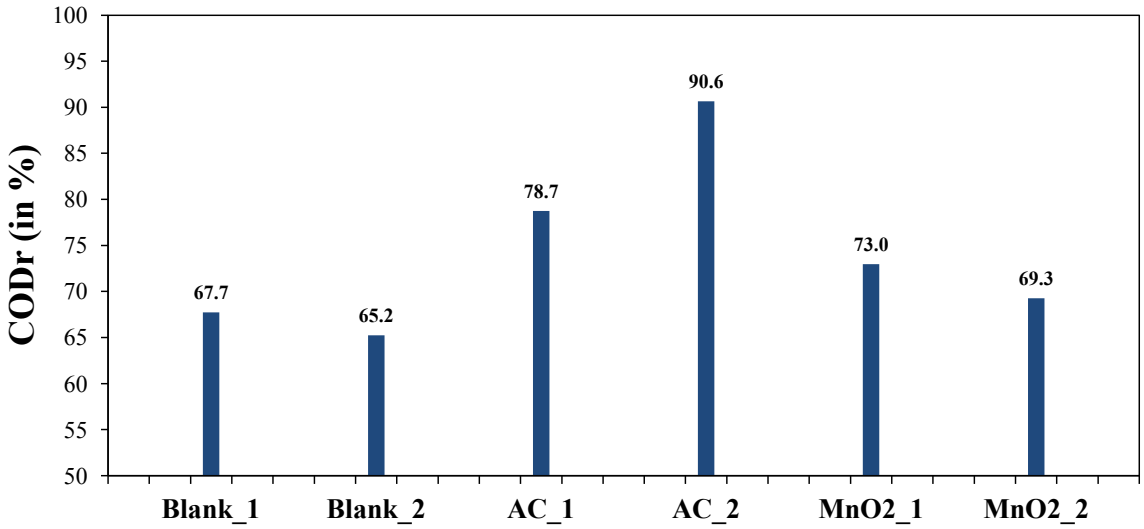

Figure 3.7: Repeat tests for blank, AC and MnO_2 (500 °C; catalyst/feed ratio: 0.1 except for AC_2!!!; reaction time: 1 h).

It can be seen that the CODr of the two repeated blank tests and the two repeated MnO_2 tests was in the same range as before. The blank tests showed a CODr of 65-68%, whereas the MnO_2 tests a CODr of 69-73%. Moreover, the CODr of one of the two repeated tests with AC also reached a similar value as before (78.7%). Interestingly, the CODr of AC_2 reached even more than 90%. The reason for this was that only about have of the feed was unwittingly put into the batch reactor. As a result, the catalyst/feed ratio was much higher (about 0.2), the gasification more successful and the CODr higher. This circumstance was figured out during the test when the reaction pressure reached only about 205-210 bar (see Appendix D.2).

3.6. Third series of tests

In the previous test series, one experiment was accidently carried out with a higher catalyst/feed ratio resulting in a higher CODr. Therefore, it was of interest to conduct further experiments with a higher catalyst/feed ratio to quantitatively determine the influence of the catalyst amount on the gasification efficiency. The tests were carried out at 500 °C with the use of AC and MnO_2 as catalysts again. The reaction time was maintained at 1 h, but the catalyst/feed ratio increased to 0.2. The CODr results of those tests are illustrated in Figure 3.8.

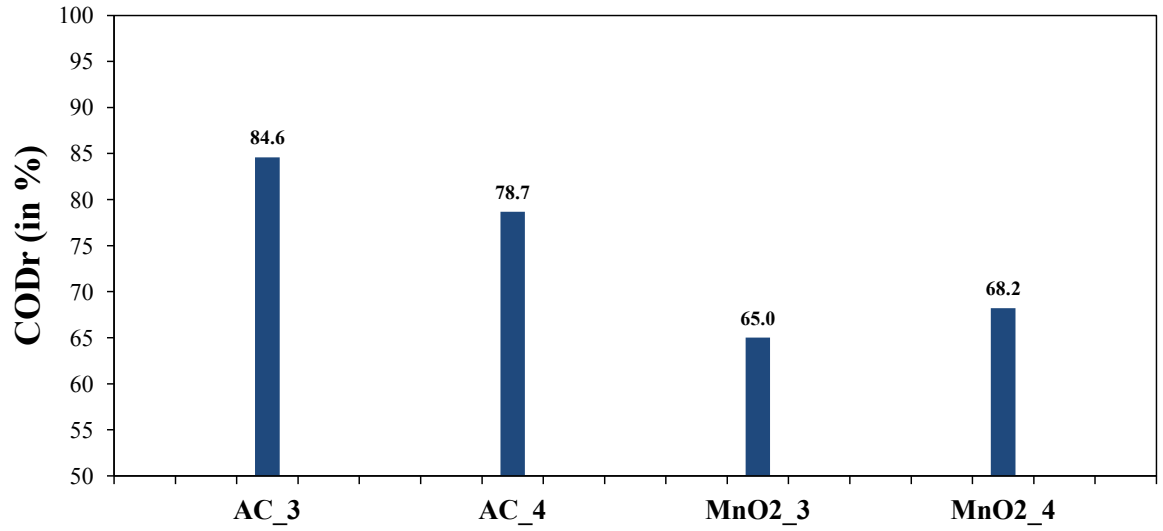

Figure 3.8: Effect of a higher catalyst amount on CODr (500 °C; catalyst/feed ratio: 0.2; reaction time: 1 h).

Contrary to the expectations, doubling the catalyst/feed ratio did not lead to significantly higher values for the CODr. One of the two tests with carbon (AC_3) led to a CODr that was a few percents higher than the CODr of the previous tests, the other one (AC_4) did not. A possible explanation for the high CODr of 90.6% with AC in the second test series (AC_2) could be that the reacting molecules were a in a gas state rather than in a supercritical state due to the low pressure ($p < p_c$), which made it easier for them to reach the surface of the carbon catalyst. Doubling the amount of the MnO_2 catalyst did not have a positive effect at all; to the contrary, it even worsened the CODr by a few percents. This conclusion could be misleading in the sense that the MnO_2 might have settled because of its high density of 5.03 g/cm^3 [61] so that the reacting molecules could not reach the entire catalyst surface. This question could only be answered with the use of a stirred batch reactor or a continuous reactor.

3.7. Fourth series of tests

To interpret and assess the results gained so far in more detail, it was decided to run additional tests with a well-known HTG catalyst. Raney-nickel was chosen because of its high activity and – compared to noble metal catalysts – low price. The experiments were carried out at 350, 400 and 500 °C with a reaction time of 1 h. The Raney-nickel catalyst was delivered as a 50/50-wt% Raney-nickel/water slurry. To have a rather too low than a too high catalyst/feed ratio, a slurry/feed ratio of 0.1 was used leading to an actual catalyst/feed ratio of 0.05. For consistency reasons, each test was run twice. The results regarding CODr are depicted in Figure 3.9.

As expected from the previous tests, the CODr increased with increasing temperature. Furthermore, Raney-nickel showed catalytic activity at each temperature since the CODr was always higher than in the corresponding blank test. Although the catalyst/feed ratio was only half of

the catalyst/feed ratio in earlier catalytic tests, the CODr reached values in the range of the tests with AC (compare Figure 3.9 with 3.3, 3.4 and 3.6). At 400 °C the CODr with Raney-nickel was even higher than the one of the AC experiment.

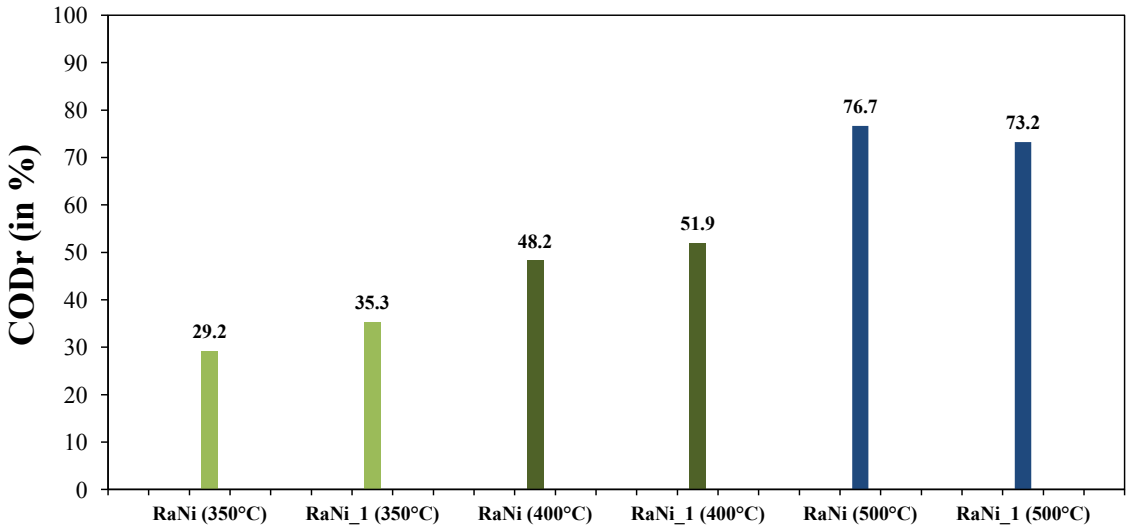

Figure 3.9: Effect of a RaNi catalyst on CODr (350 °C, 400 °C, 500 °C; catalyst/feed ratio: 0.05; reaction time: 1 h).

In comparison, Elliott *et al.* [62] were able to reach a carbon gasification efficiency of 93% after treatment of a 10 wt% p-cresol solution for 90 min at 350 °C and 200 bar with Raney-nickel (no catalyst/feed ratio stated). Afif *et al.* [63] reached a carbon gasification efficiency of 69% when gasifying a 3 wt% activated sludge solution for 15 min at 380 °C (1.8 g_{RaNi}/g_{Sludge}). Waldner *et al.* [52] were able to reach complete carbon gasification through HTG of sawdust slurries (< 30 wt%) for 90 min over RaNi (0.5 $g_{RaNi}/g_{Sawdust}$) at around 400 °C and 300 bar. Finally, Guo *et al.* [28] reached a CODr of 96.2% when gasifying a 7.8 wt% black liquor solution for 10 min over RaNi (0.1 g_{RaNi}/g_{Liquor}) at 500 °C.

3.8. Fifth series of tests

Although a lot of experiments had been performed, no acceptably high CODr could be reached so far. The previous tests showed that an increase in temperature significantly increased the CODr. Therefore, it was decided to go one step further and carry out experiments at 600 °C. Blank tests and catalytic tests with AC, MnO_2 and Raney-Ni were conducted. As before, the reaction time was 1 h and the catalyst/feed ratio 0.1 for AC and MnO_2 and 0.05 for Raney-nickel, respectively. Each test was run twice for consistency reasons. To be mentioned at this point, the fact that 600 °C is above the flash point of MnO_2 (535 °C, [61]) was figured out after the experiments. However, no special behavior/result was observed during or after the tests. The CODr results for the experiments conducted at 600 °C are showed in Figure 3.10.

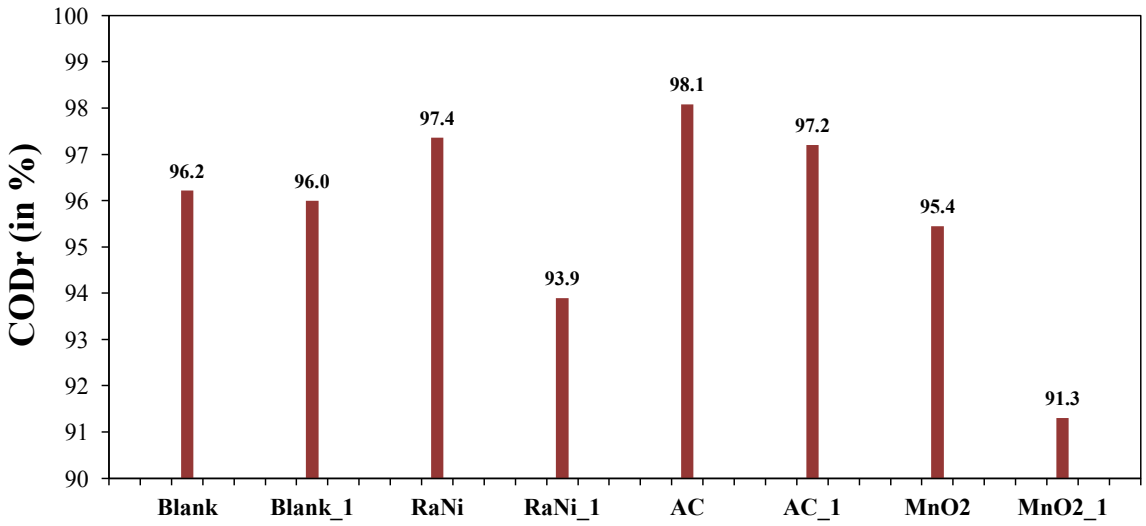

Figure 3.10: Effect of catalysts on CODr at high temperature (600 °C; catalyst/feed ratio: 0.1 for AC and Mn_2, 0.05 for RaNi; reaction time: 1 h).

It can be seen that the CODr increased a lot and reached values above 90% in all tests. The CODr was the lowest for the tests with MnO_2. It seems that MnO_2 had a small inhibitory effect on the gasification, which might have had something to do with the temperature having been above the flash point of MnO_2. The CODr of the blank tests reached even more than 96%; however, some coke was produced (see Figure 3.2d). In how far coke was generated in the catalytic tests, too, could be only determined by analysis of spent catalysts, which was not included in the course of this project. The highest CODr of 97-98% was reached with AC. In comparison, Xu *et al.* [36] reached a carbon gasification efficiency of 95-100% through continuous HTG of a 1.2 M glucose solution over AC and charcoal derived from different sources with a WHSV of 12.6-25.7 h^{-1} at 600 °C and 345 bar.

In addition, the pH values of our examples were in the range of 8-9, which might have been related to the formation of ammonia [15].

4. Summary and recommendations

4.1. Summary of the experiments

- Catalytic and non-catalytic tests regarding HTG of HTL wastewater were carried out. The tests were performed in a 20.1 mL tubular batch reactor at 350-600 °C and 220-340 bar with a reaction time of 1 h. AC (activated carbon), α-Al_2O_3, TiO_2 (rutile), diatomaceous earth (DE), MnO_2 and Raney-nickel were assessed for their suitability as heterogeneous catalysts.
- The CODr (COD removal efficiency) increased with temperature independent from the use of a catalyst.
- The higher the CODr was, the clearer became the liquid product.
- AC and Raney-nickel showed the highest catalytic activities.
- Al_2O_3, TiO_2 and DE did not have any catalytic effect in the temperature range of 350-500 °C. TiO_2 and DE even seemed to have an inhibitory influence on the CODr.
- Doubling the amount of AC and MnO_2 did not result in significantly higher values for the CODr. Settling of the catalyst might have prevented the molecules from reaching the entire catalytic surface.
- The CODr of the tests with Raney-nickel was as high as the one of the corresponding AC tests, although the catalyst/feed ratio was only half as high.
- The highest COD removal efficiencies could be reached at 600 °C. The CODr of the blank tests was around 96%, the one of the Raney-nickel tests in the range of 93.9-97.4% and the one of the AC-catalyzed tests in the range of 97.2-98.1%. However, in the case of the blank tests, coke production was observed.
- The pH of the liquid phases after treatment at 600 °C was in the range of 8-9 very likely due to the formation of ammonia.

4.2. Recommendations for future work

Based on the experience gained from the tests and literature review, the following recommendations should be considered:

- The most promising and interesting experiments should be repeated for better reproducibility.
- Additional tests using different reaction times and catalyst/feed ratios should be conducted to get a deeper understanding of the relationships and processes taking place.

- Gas analysis would deliver very valuable information. If it turns out that at a certain temperature and/or with a certain catalyst H_2 is the favored product rather than CH_4, HTG of HTL wastewater might be an interesting way to produce H_2, which is needed for hydrotreatment of the bio-crude gained from HTL [Elliott2015].
- Further tests with different HTL wastewaters (e.g. from HTL of algae, municipal waste) should be performed to determine the general validity of the results of this project.
- Other catalysts, which might be more active at lower temperatures (350-500 °C), should be tested.
- If possible, tests at even higher temperatures could be run. Maybe at 650 °C complete gasification without a catalyst is possible.
- Continuous tests have to be conducted to assess catalyst- and process stability. Moreover, they would better show the influence of the catalyst amount on the gasification efficiency and the CODr.
- When moving from batch- to continuous mode, aspects like catalyst poisoning [47, 48], corrosion [51] and plugging through coke deposition [51] and salt precipitation [64] have to be considered.
- Finally, a profitability analysis should be conducted. Especially heat integration will play an important role for making the process feasible [65, 66].

A. Batch reactor parts

Table A.1: Swagelok parts of the batch reactors.

Component	Product number
Reactor cap	SS-810-C
Reactor tubing	SS-T8-S-083-20
Reducer (reactor, capillary)	SS-810-6-2
Capillary	SS-T2-S-035-6ME
Reducer (capillary, T-piece)	SS-200-R-4
T-piece	SS-400-3-4TFT
Pressure gauge	PGN-50-CNG400-LAQ
High-pressure valve	SS-1VM4-S4-BKB
Plug	SS-400-P

B. Catalysts

Table B.1: Catalysts used for the experiments.

Catalyst	CAS number	Supplier	Product name/number
Activated carbon (powder)	7440-44-0	unknown	DARCO® ULTRA 100
Aluminum oxide	1344-28-1	Sigma-Aldrich®	342653
Titanium oxide	1317-80-2	Sigma-Aldrich®	637262
Manganese oxide	1313-13-9	Sigma-Aldrich®	243442
Diatomaceous Earth	-	unknown	Dterra™ NutriDE™
Raney®-Nickel	7440-02-0	Sigma-Aldrich®	221678

C. GC-MS results

Table C.1: Results gained from GC-MS analysis of the feed.

Compound	Retention time (in min)	Area	Relative peak area (in %)
Pyrazine	6.69	11302323	1.46
PYRAZINE, METHYL-	8.18	60971865	7.89
Pyrazine, 2,5-dimethyl-	9.72	14472884	1.87
PYRAZINE, ETHYL-	9.93	18977128	2.45
PYRAZINE, ETHYL-	9.94	10732945	1.39
PYRAZINE, 2,3-DIMETHYL-	10.38	7218705	0.93
2-Cyclopenten-1-one, 2-methyl-	10.86	4847897	0.63
Pyrazine, 2-ethyl-5-methyl-	11.31	7443994	0.96
Pyrazine, 2-ethyl-5-methyl-	11.92	3527877	0.46
Pyrazine, 2-ethyl-5-methyl-	12.89	2908903	0.38
2-CYCLOPENTEN-1-ONE, 2-METHYL-	14.76	4224351	0.55
2-Cyclopenten-1-one, 2,3-dimethyl-	15.20	4341926	0.56
Propanoic acid	15.43	62051043	8.03
Propanoic acid, 2-methyl-	16.24	16053929	2.08
2-Cyclopenten-1-one, 3-ethyl-	17.27	1056188	0.14
BUTYRIC ACID	17.55	185190261	23.95
Butonic acid, 3-methyl (IS)	18.54	37270921	4.82
Butanamide, N-ethyl-	19.81	3911212	0.51
PENTANOIC ACID	20.04	43627837	5.64
ACETAMIDE	20.77	29556220	3.82
Pentanoic acid, 4-methyl-	21.38	10039497	1.30
Propanamide	21.60	12540592	1.62
PYRROLIDINE, 1-ACETYL-	21.78	10929026	1.41
Hexanoic acid	22.23	15433945	2.00
Phenol, 2-methoxy-	22.38	6271601	0.81
N-(3-Methylbutyl)acetamide	22.66	3346112	0.43
2,5-Pyrrolidinedione, 1-ethyl-	22.75	3506307	0.45
BUTANAMIDE	23.19	25701898	3.32
Butanoic acid, pyrrolidide	23.52	2464409	0.32
BUTANAMIDE, 3-METHYL-	23.68	2200771	0.28
1-(1H-PYRROL-2-YL)ETHANONE	24.56	2414485	0.31
Phenol	25.29	9323151	1.21
2-Pyrrolidinone	25.74	21465415	2.78
Phenol, 4-methyl-	26.72	3972653	0.51
2-Piperidinone	27.38	24879086	3.22
3-Pyridinol, 2,6-dimethyl-	30.16	3802803	0.49
3-PYRIDINOL, 2-METHYL-	30.52	10151733	1.31
Glycerin	30.74	4327918	0.56
4-Amino-2-hydroxytoluene	31.16	5304897	0.69
3-PYRIDINOL, 6-METHYL-	32.10	9046230	1.17
3-Pyridinol	32.41	43274014	5.60
ACETAMIDE, N-(2-PHENYLETHYL)-	34.93	3183289	0.41
Benzenepropanoic acid	35.51	3183562	0.41
CYCLO(L-PROLYL-L-PROLYL)	43.43	5003343	0.65
Tyramine, N-formyl-	50.79	1639734	0.21

D. Progressions of temperature and pressure

D.1. First series of tests

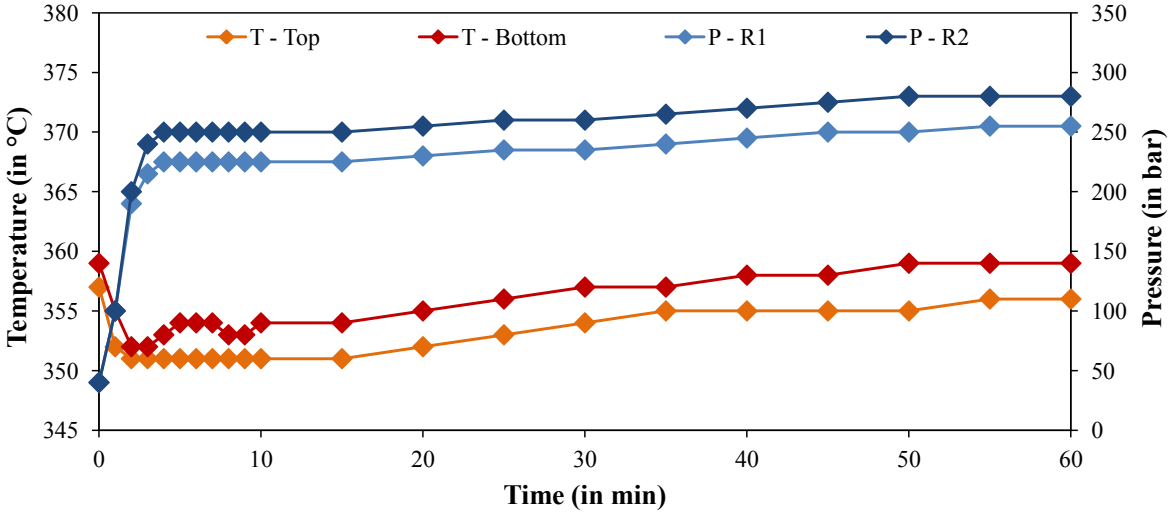

Figure D.1: R1: Blank, R2: AC (350 °C).

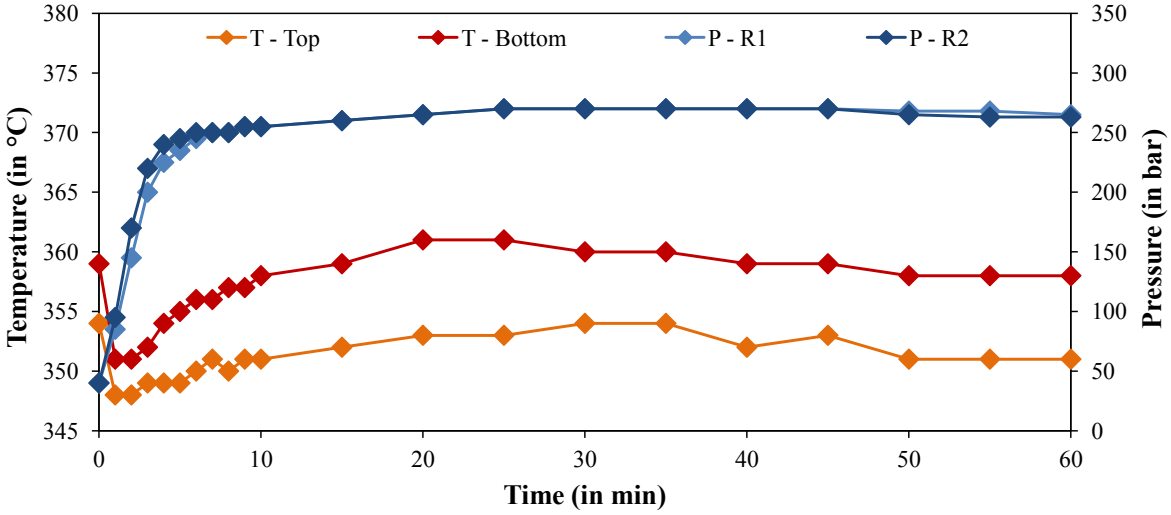

Figure D.2: R1: Al_2O_3, R2: TiO_2 (350 °C).

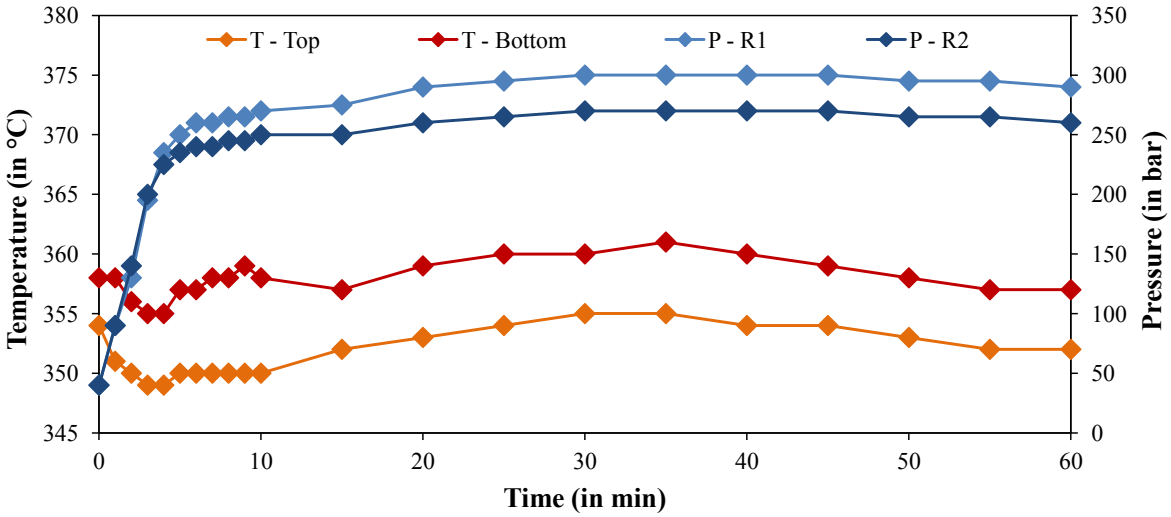

Figure D.3: R1: DE, R2: MnO_2 (350 °C).

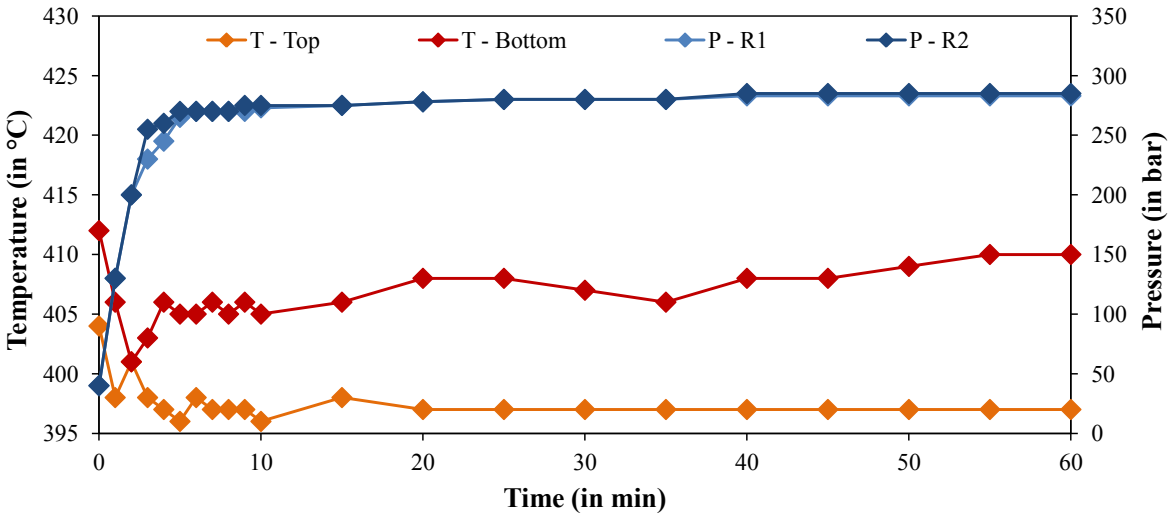

Figure D.4: R1: Blank, R2: AC (400 °C).

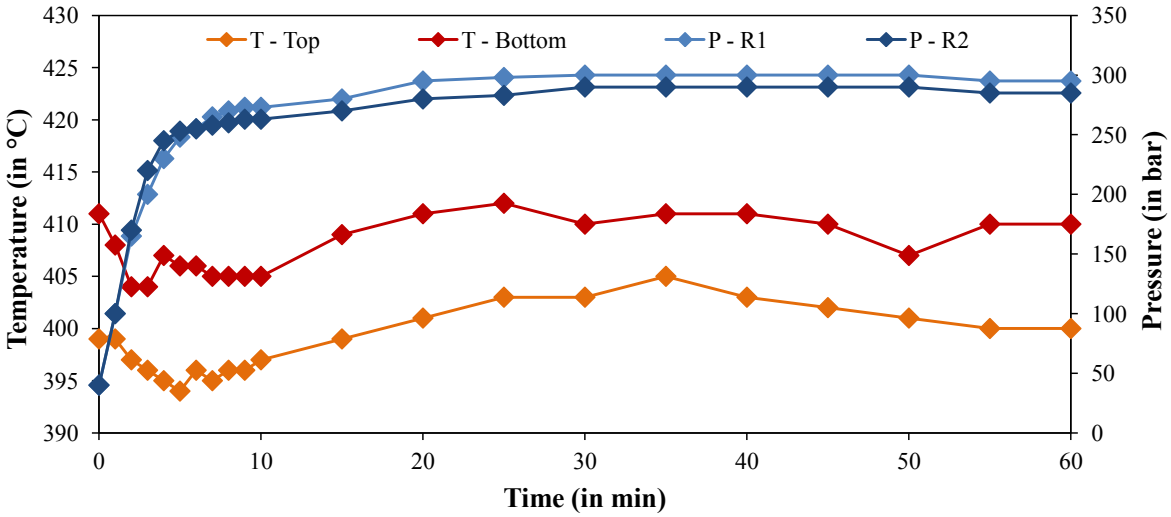

Figure D.5: R1: Al_2O_3, R2: TiO_2 (400 °C).

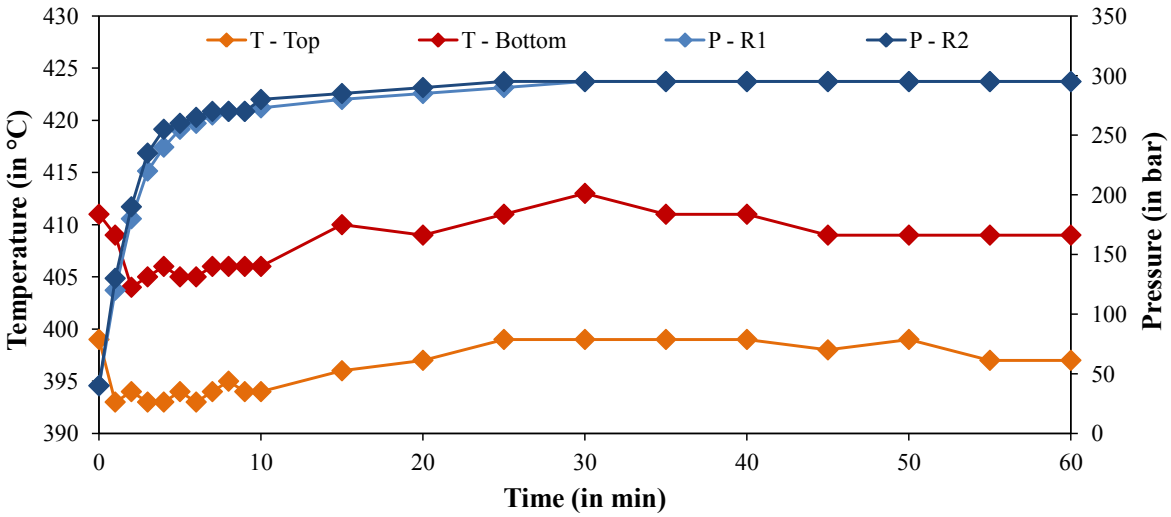

Figure D.6: R1: DE, R2: MnO_2 (400 °C).

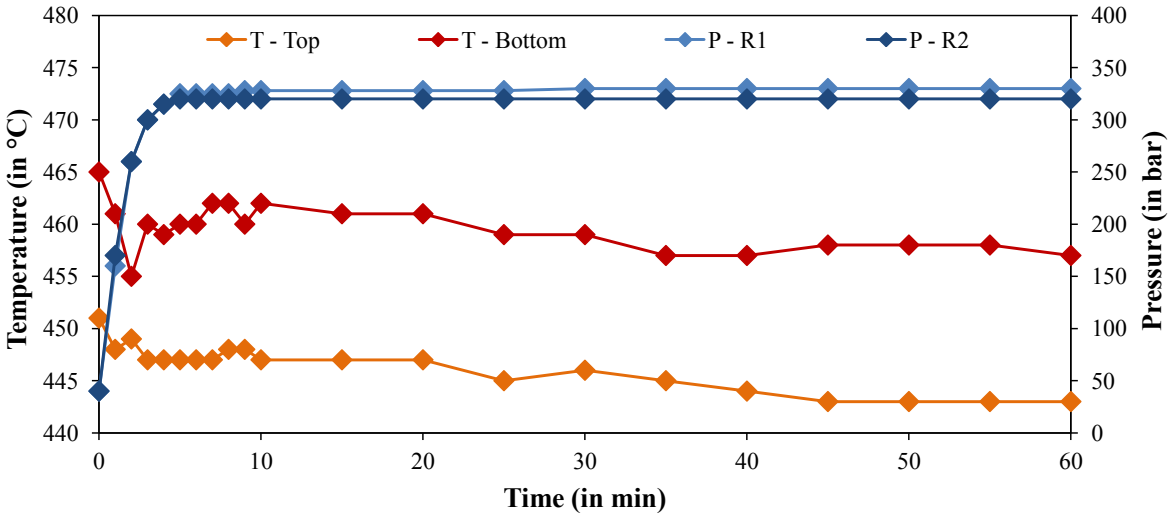

Figure D.7: R1: Blank, R2: AC (450 °C).

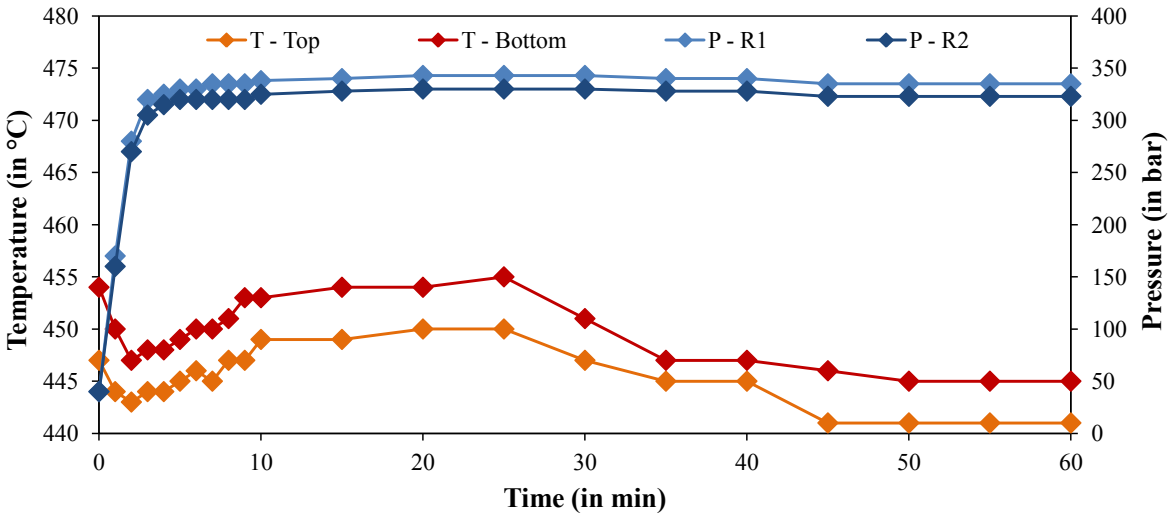

Figure D.8: R1: Al_2O_3, R2: TiO_2 (450 °C).

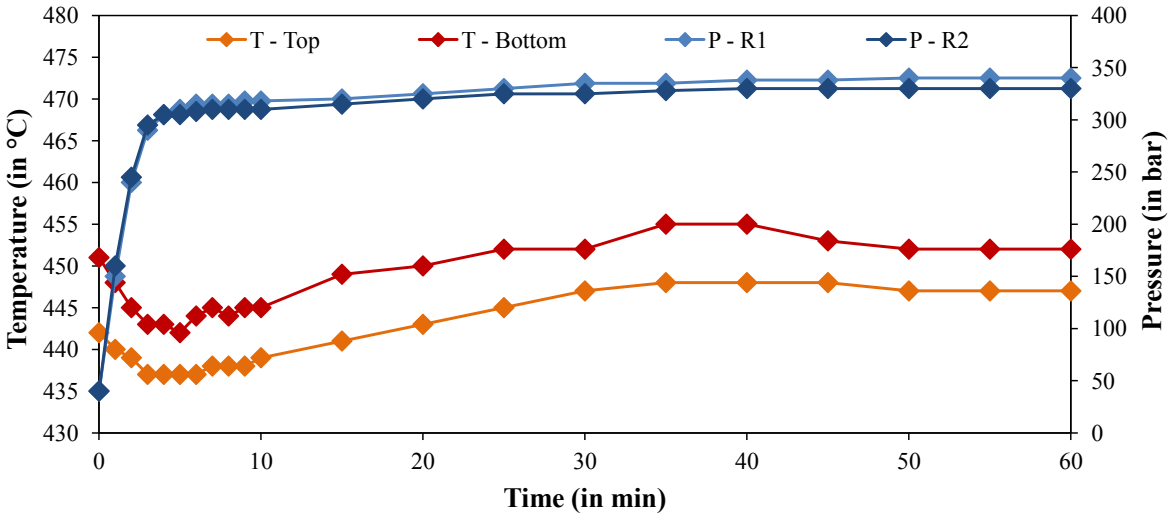

Figure D.9: R1: DE, R2: MnO_2 (450 °C).

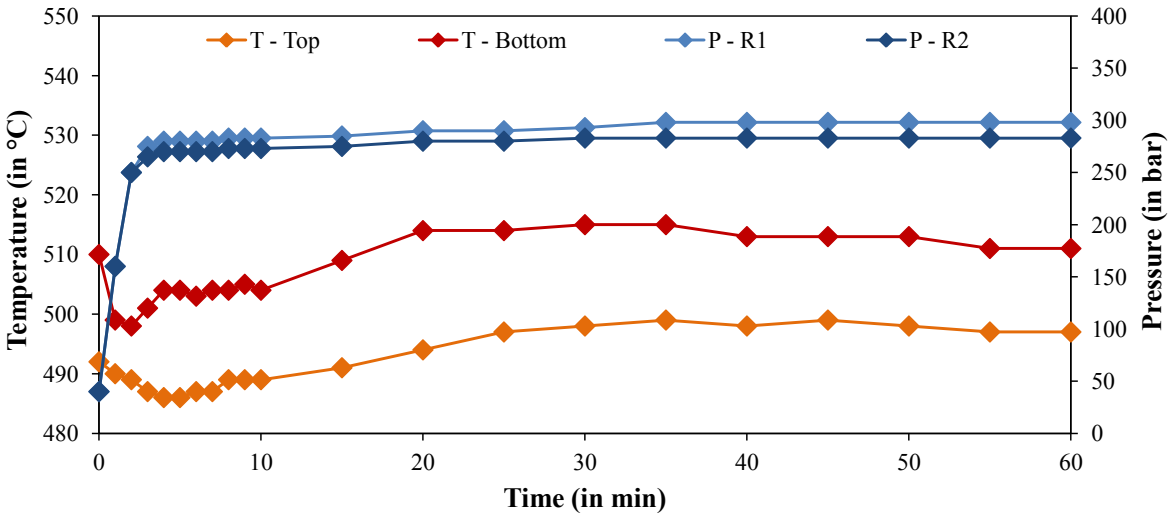

Figure D.10: R1: Blank, R2: AC (500 °C).

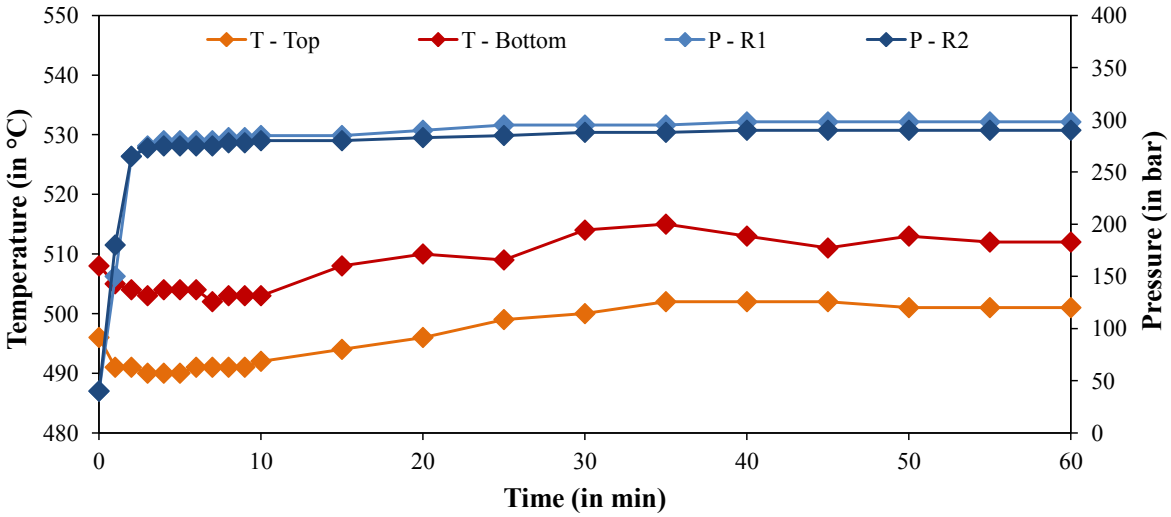

Figure D.11: R1: Al_2O_3, R2: TiO_2 (500 °C).

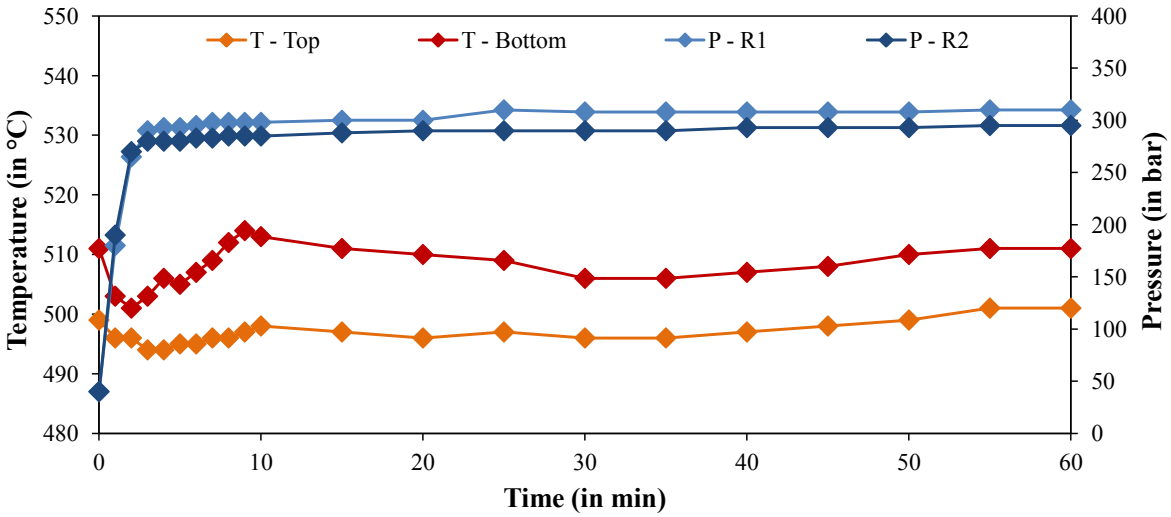

Figure D.12: R1: DE, R2: MnO_2 (500 °C).

D.2. Second series of tests

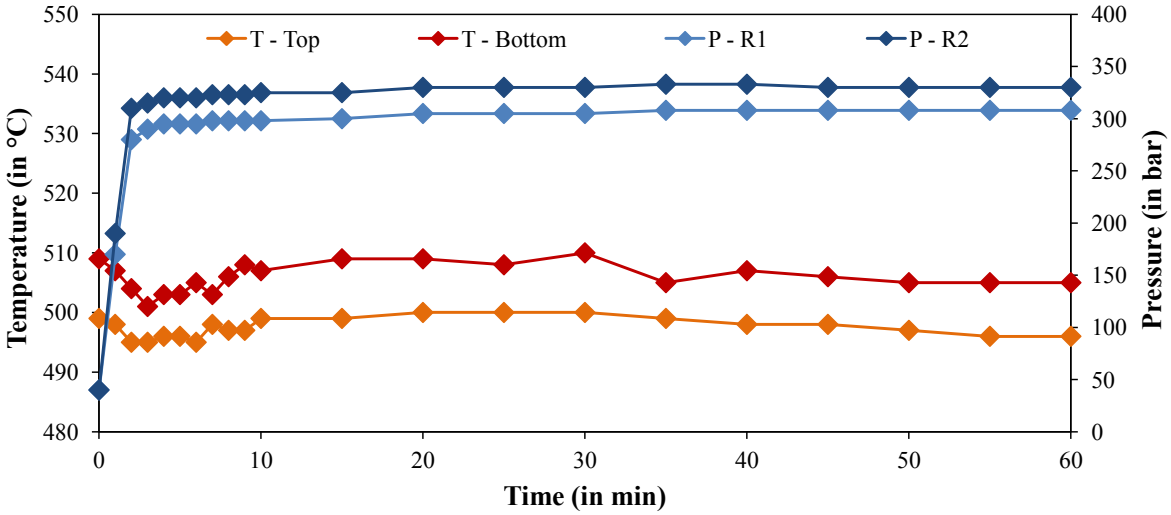

Figure D.13: R1: Blank_1, R2: Blank_2 (500 °C).

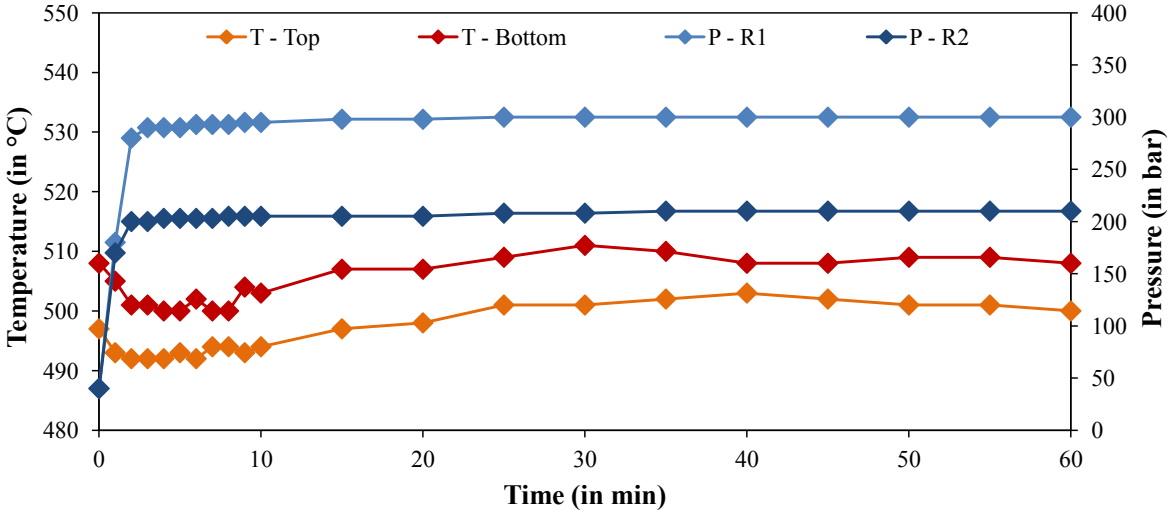

Figure D.14: R1: AC_1, R2: AC_2 (500 °C).

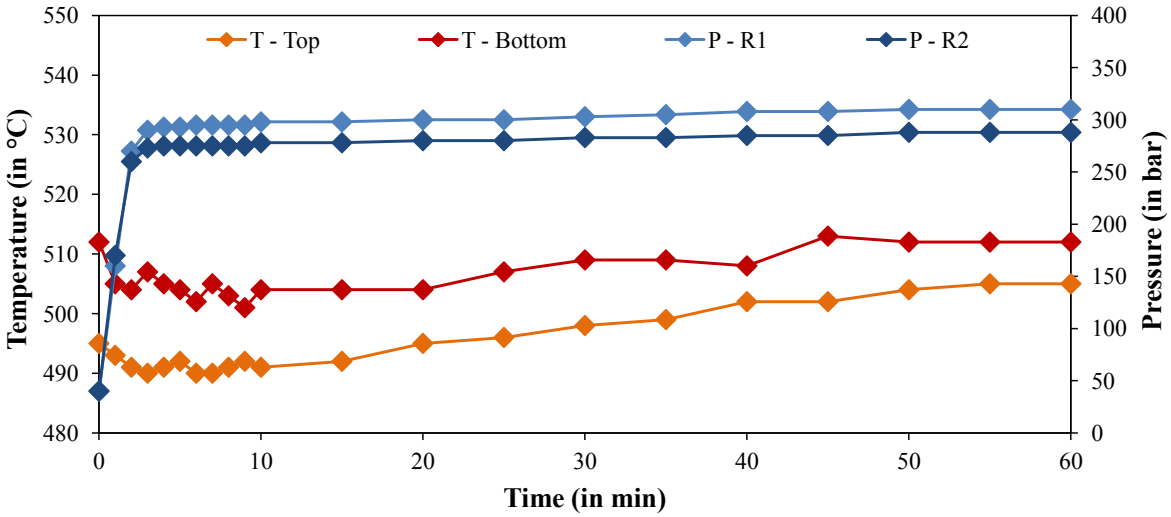

Figure D.15: R1: MnO_2_1, R2: MnO_2_2 (500 °C).

D.3. Third series of tests

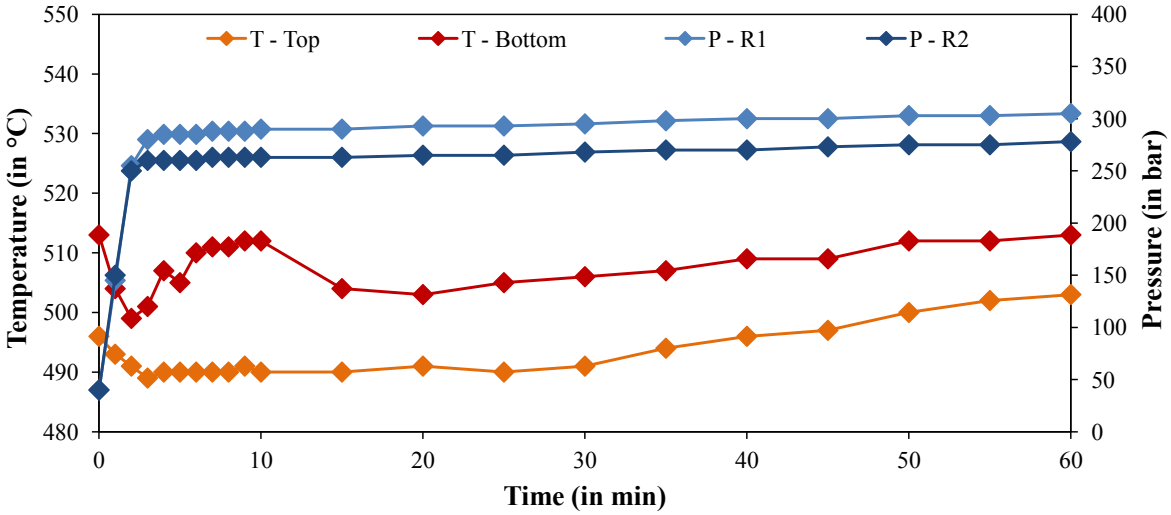

Figure D.16: R1: AC_3, R2: AC_4 (500 °C).

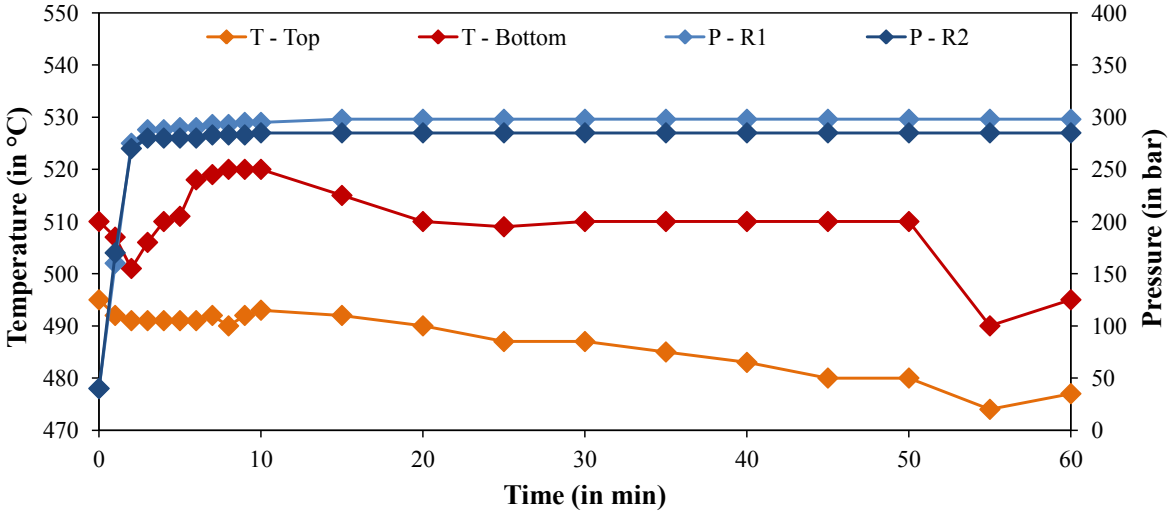

Figure D.17: R1: MnO_2_3, R2: MnO_2_4 (500 °C).

D.4. Fourth series of tests

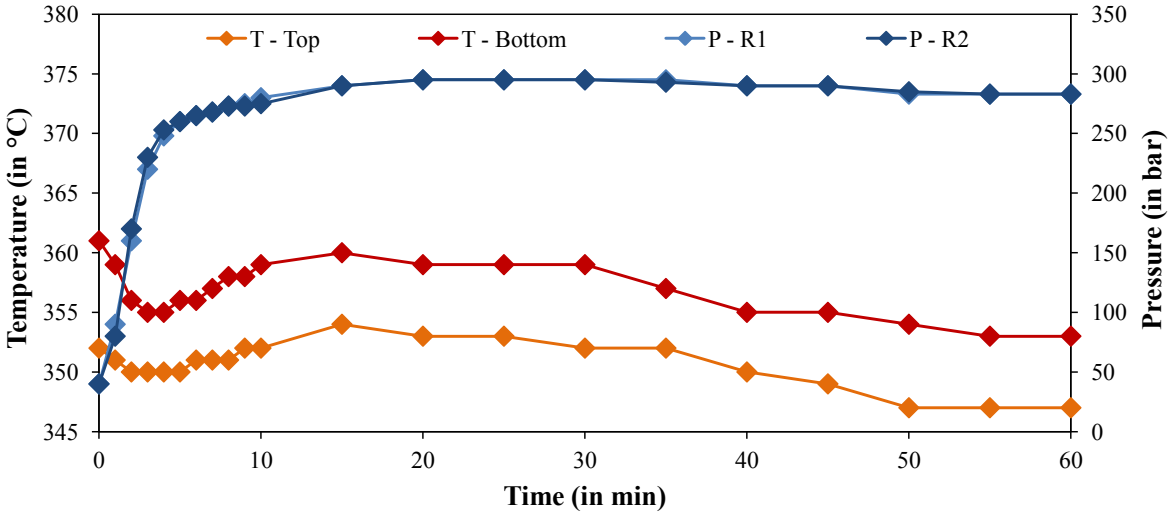

Figure D.18: R1: RaNi, R2: RaNi_1 (350 °C).

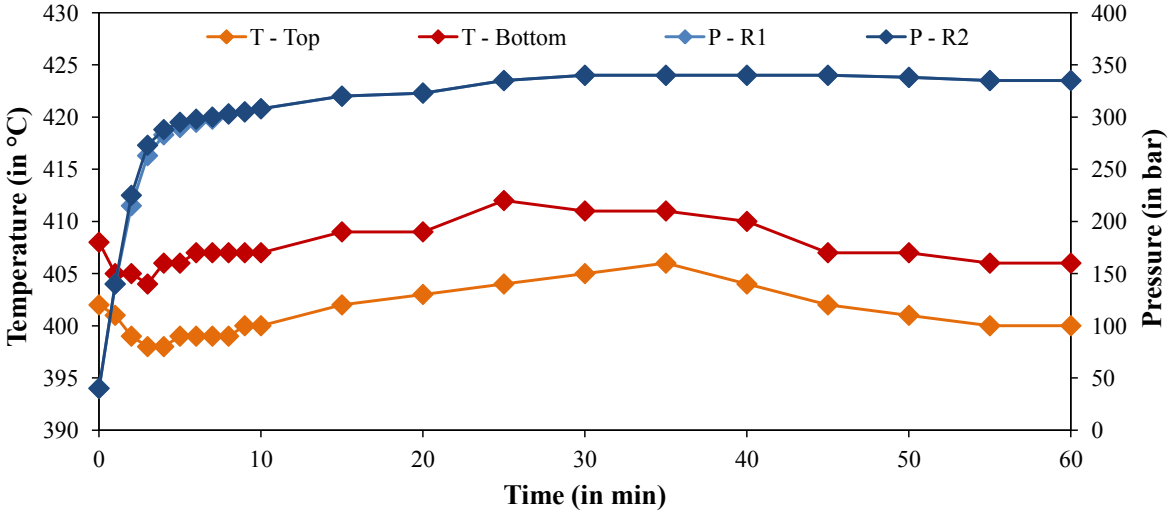

Figure D.19: R1: RaNi, R2: RaNi_1 (400 °C).

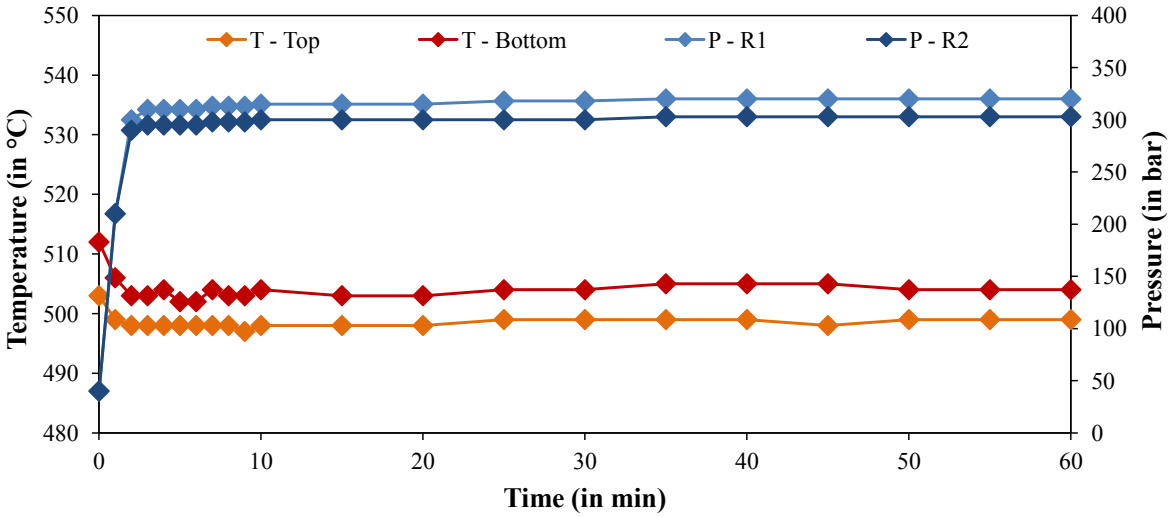

Figure D.20: R1: RaNi, R2: RaNi_1 (500 °C).

D.5. Fifth series of tests

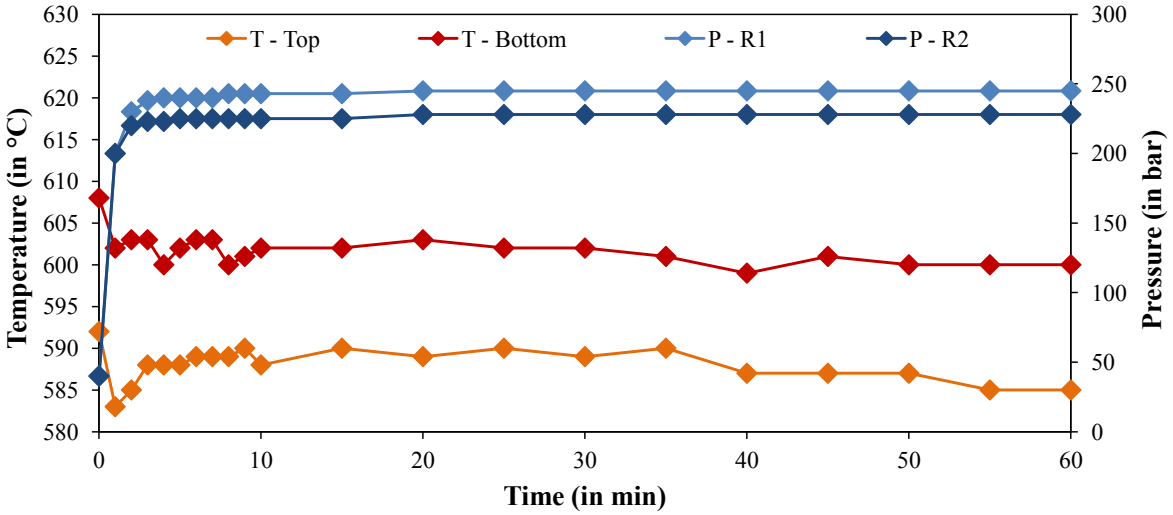

Figure D.21: R1: Blank, R2: Blank_1 (600 °C).

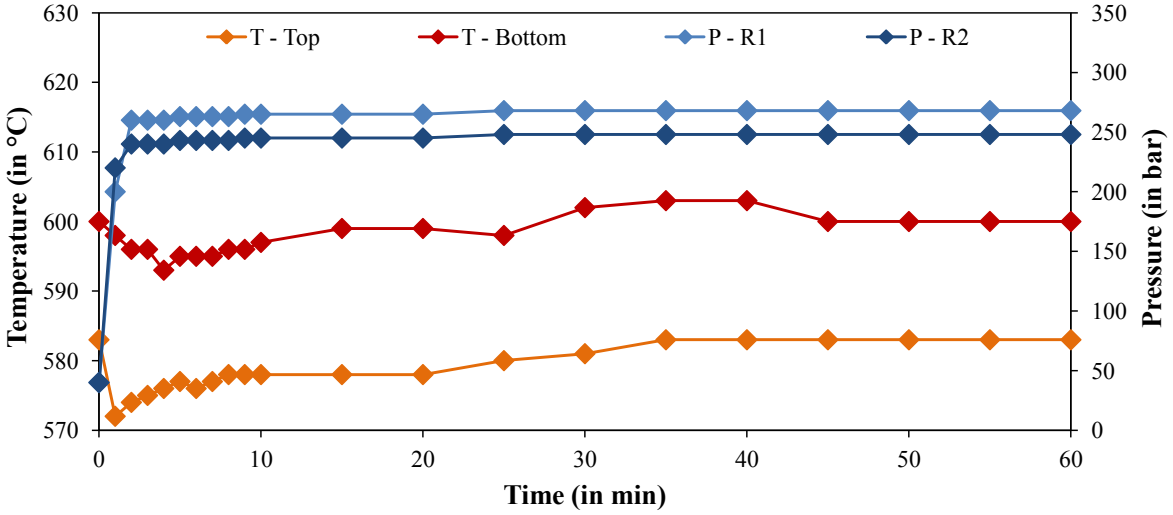

Figure D.22: R1: RaNi, R2: RaNi_1 (600 °C).

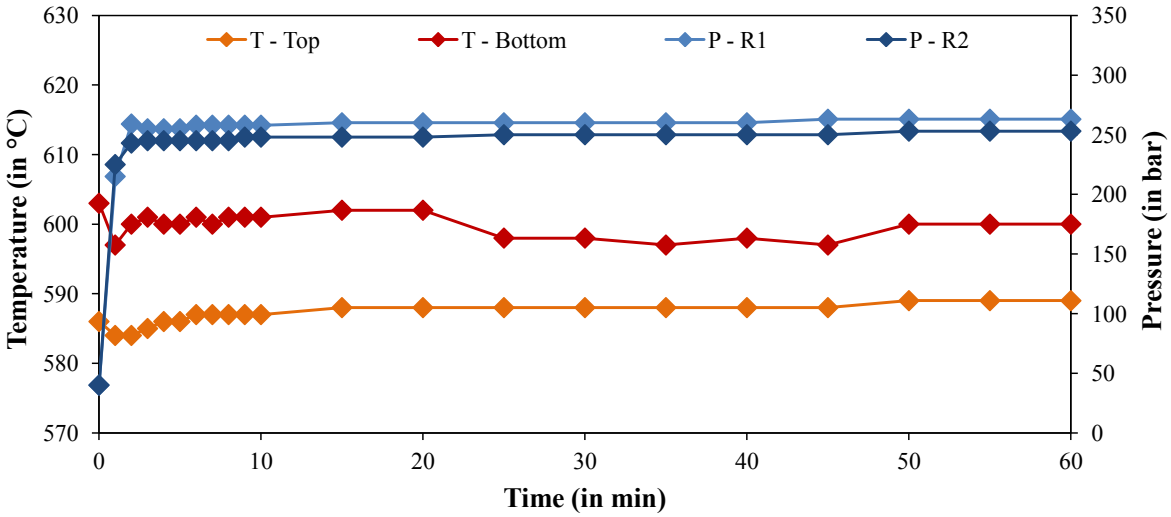

Figure D.23: R1: AC, R2: AC_1 (600 °C).

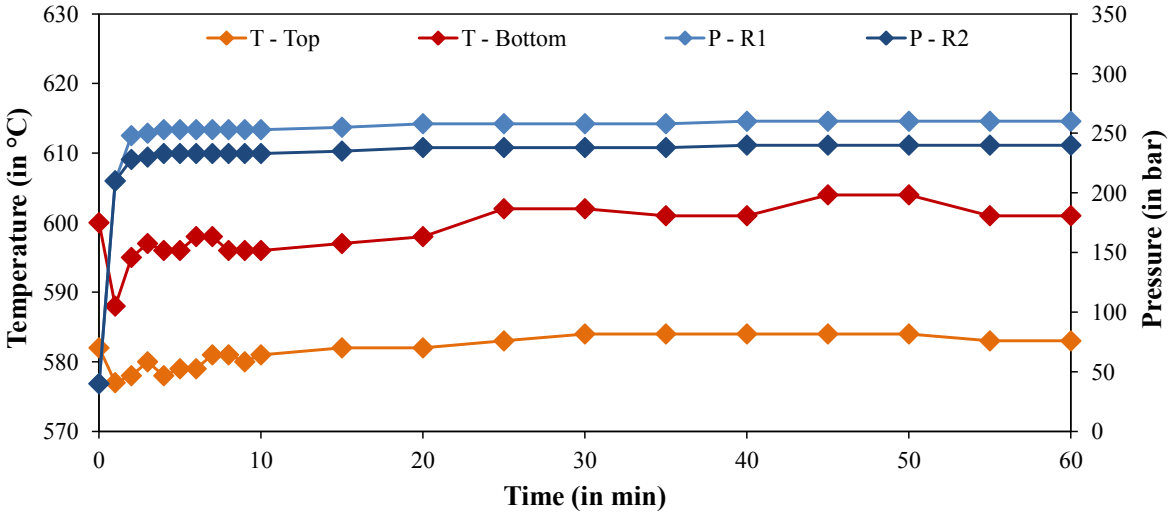

Figure D.24: R1: MnO_2, R2: MnO_2_1 (600 °C).

E. COD results

E.1. First series of tests

Table E.1: COD data of the first series of tests.

Reaction temperature (in °C)	Catalyst	Catalyst/feed ratio (in g/g)	CODr (in %)	SD
350	Blank	-	17.12	0.00
350	AC	0.1	37.01	0.00
350	Al_2O_3	0.1	17.84	0.45
350	TiO_2	0.1	17.12	0.21
350	DE	0.1	15.63	1.21
350	MnO_2	0.1	19.33	0.16
400	Blank	-	18.19	0.48
400	AC	0.1	35.94	0.61
400	Al_2O_3	0.1	19.67	0.48
400	TiO_2	0.1	21.67	0.37
400	DE	0.1	18.77	0.36
400	MnO_2	0.1	29.41	0.32
450	Blank	-	36.94	2.47
450	AC	0.1	47.82	0.16
450	Al_2O_3	0.1	40.84	0.89
450	TiO_2	0.1	32.59	0.32
450	DE	0.1	29.86	0.65
450	MnO_2	0.1	41.53	0.59
500	Blank	-	69.78	0.51
500	AC	0.1	76.76	0.06
500	Al_2O_3	0.1	69.13	0.41
500	TiO_2	0.1	64.91	0.22
500	DE	0.1	64.19	0.42
500	MnO_2	0.1	71.09	0.27

E.2. Second series of tests

Table E.2: COD data of the second series of tests.

Reaction temperature (in °C)	Catalyst	Catalyst/feed ratio (in g/g)	CODr (in %)	SD
500	Blank_1	0.1	64.39	0.47
500	Blank_2	0.1	65.22	0.47
500	AC_1	0.1	78.73	0.32
500	AC_2	> 0.1	90.64	0.16
500	MnO_2_1	0.1	72.96	0.68
500	MnO_2_2	0.1	69.26	0.24

E.3. Third series of tests

Table E.3: COD data of the third series of tests.

Reaction temperature (in °C)	Catalyst	Catalyst/feed ratio (in g/g)	CODr (in %)	SD
500	AC_3	0.2	84.60	0.39
500	AC_4	0.2	78.69	0.39
500	MnO_2_3	0.2	65.02	0.32
500	MnO_2_4	0.2	68.19	0.89

E.4. Fourth series of tests

Table E.4: COD data of the fourth series of tests.

Reaction temperature (in °C)	Catalyst	Catalyst/feed ratio (in g/g)	CODr (in %)	SD
350	RaNi	0.05	29.69	7.09
350	RaNi_1	0.05	35.28	7.09
400	RaNi	0.05	48.23	0.26
400	RaNi_1	0.05	51.93	1.35
500	RaNi	0.05	76.65	0.83
500	RaNi_1	0.05	73.24	1.20

E.5. Fifth series of tests

Table E.5: COD data of the fifth series of tests.

Reaction temperature (in °C)	Catalyst	Catalyst/feed ratio (in g/g)	CODr (in %)	SD
600	Blank	-	96.44	0.24
600	Blank_1	-	95.99	0.24
600	RaNi	0.05	96.20	2.00
600	RaNi_1	0.05	93.89	0.63
600	AC	0.1	98.17	0.39
600	AC_1	0.1	97.20	0.18
600	MnO_2	0.1	94.89	0.98
600	MnO_2_1	0.1	91.30	0.21

F. Valve issue

The valves that were used for the experiments (see Appendix A) were not the ones of first choice. Initially, other valves were purchased (Swagelok, SS-BVM4-SH), which were believed to be the most suitable and robust ones. However, it turned out that gas could also exit through the threads of the valve during depressurization of the reactor because it had no packing. This would have been disadvantageous if a product gas had to be collected. Therefore, another type (Swagelok, SS-3HNRS4-G) was ordered, but it would have taken two months for delivery. Fortunately, a third type (the one actually used) was found in the lab with pressure- and temperature ratings just high enough for the experiments.

References

[1] International Energy Agency, editor. *Key World Energy Statistics*. 2014.

[2] ESRL Web Team et al. ESRL Global Monitoring Division, http://www.esrl.noaa.gov/gmd/ccgg/trends/ (retrieved February 19, 2015).

[3] Stocker and D Qin. Climate change 2013: The physical science basis. *Working Group I Contribution to the Fifth Assessment Report of the Intergovernmental Panel on Climate Change, Summary for Policymakers, IPCC*, 2013.

[4] A Kruse and A Gawlik. Biomass conversion in water at 330-410 c and 30-50 mpa. identification of key compounds for indicating different chemical reaction pathways. *Industrial & Engineering Chemistry Research*, 42(2):267–279, 2003.

[5] Frédéric Vogel. Catalytic conversion of high-moisture biomass to synthetic natural gas in supercritical water. *Handbook of Green Chemistry*, 2009.

[6] Andrea Kruse. Supercritical water gasification. *Biofuels, Bioproducts and Biorefining*, 2(5):415–437, 2008.

[7] E.W. Lemmon, M.O. McLinden, and D.G. Friend. *"Thermophysical Properties of Fluid Systems" in NIST Chemistry WebBook, NIST Standard Reference Database Number 69*. Eds. P.J. Linstrom and W.G. Mallard, National Institute of Standards and Technology, Gaithersburg MD, 20899, http://webbook.nist.gov, (retrieved April 05, 2014).

[8] AD Chistyakov. The permittivity of water and water vapor in saturation states. *Russian Journal of Physical Chemistry*, 81(1):5–8, 2007.

[9] DP Fernandez, ARH Goodwin, Eric W Lemmon, JMH Levelt Sengers, and RC Williams. A formulation for the static permittivity of water and steam at temperatures from 238 k to 873 k at pressures up to 1200 mpa, including derivatives and debye–hückel coefficients. *Journal of Physical and Chemical Reference Data*, 26(4):1125–1166, 1997.

[10] Jefferson W Tester, Philip A Marrone, Matthew M DiPippo, Kentaro Sako, Matthew T Reagan, Tomas Arias, and William A Peters. Chemical reactions and phase equilibria of model halocarbons and salts in sub-and supercritical water (200–300 bar, 100–600 c). *The Journal of supercritical fluids*, 13(1):225–240, 1998.

[11] W. M. Haynes. *CRC Handbook of Chemistry and Physics, 94th Edition (Internet Version 2014)*. CRC Press/Taylor and Francis, Boca Raton, FL.

[12] Andrei V Bandura and Serguei N Lvov. The ionization constant of water over wide ranges of temperature and density. *Journal of physical and chemical reference data*, 35(1):15–30, 2005.

[13] W Bühler, E Dinjus, HJ Ederer, A Kruse, and C Mas. Ionic reactions and pyrolysis of glycerol as competing reaction pathways in near-and supercritical water. *The Journal of Supercritical Fluids*, 22(1):37–53, 2002.

[14] Andrew A Peterson, Frédéric Vogel, Russell P Lachance, Morgan Fröling, Michael J Antal Jr, and Jefferson W Tester. Thermochemical biofuel production in hydrothermal media: a review of sub-and supercritical water technologies. *Energy & Environmental Science*, 1(1):32–65, 2008.

[15] Douglas C Elliott, Patrick Biller, Andrew B Ross, Andrew J Schmidt, and Susanne B Jones. Hydrothermal liquefaction of biomass: Developments from batch to continuous process. *Bioresource technology*, 178:147–156, 2015.

[16] Mitsumasa Osada, Takafumi Sato, Masaru Watanabe, Masayuki Shirai, and Kunio Arai. Catalytic gasification of wood biomass in subcritical and supercritical water. *Combustion Science and Technology*, 178(1-3):537–552, 2006.

[17] Julia L Faeth, Peter J Valdez, and Phillip E Savage. Fast hydrothermal liquefaction of nannochloropsis sp. to produce biocrude. *Energy & Fuels*, 27(3):1391–1398, 2013.

[18] Yuanhui Zhang. Hydrothermal liquefaction to convert biomass into crude oil. *Biofuels from agricultural wastes and byproducts*, page 201, 2010.

[19] Christian Stevens and Robert C Brown. *Thermochemical processing of biomass: conversion into fuels, chemicals and power*, volume 12. John Wiley & Sons, 2011.

[20] A Kruse and E Dinjus. Hot compressed water as reaction medium and reactant: properties and synthesis reactions. *The Journal of Supercritical Fluids*, 39(3):362–380, 2007.

[21] Saqib Sohail Toor, Lasse Rosendahl, and Andreas Rudolf. Hydrothermal liquefaction of biomass: a review of subcritical water technologies. *Energy*, 36(5):2328–2342, 2011.

[22] P Biller and AB Ross. Potential yields and properties of oil from the hydrothermal liquefaction of microalgae with different biochemical content. *Bioresource technology*, 102(1):215–225, 2011.

[23] Wan-Ting Chen, Yuanhui Zhang, Jixiang Zhang, Guo Yu, Lance C Schideman, Peng Zhang, and Mitchell Minarick. Hydrothermal liquefaction of mixed-culture algal biomass from wastewater treatment system into bio-crude oil. *Bioresource technology*, 152:130–139, 2014.

[24] KS Ocfemia, Y Zhang, T Funk, et al. Hydrothermal processing of swine manure into oil using a continuous reactor system: Development and testing. *Transactions of the ASABE*, 49(2):533–541, 2006.

[25] Christopher Jazrawi, Patrick Biller, Andrew B Ross, Alejandro Montoya, Thomas Maschmeyer, and Brian S Haynes. Pilot plant testing of continuous hydrothermal liquefaction of microalgae. *Algal Research*, 2(3):268–277, 2013.

[26] N Boukis, V Diem, W Habicht, and E Dinjus. Methanol reforming in supercritical water. *Industrial & Engineering Chemistry Research*, 42(4):728–735, 2003.

[27] Sivamohan N Reddy, Sonil Nanda, Ajay K Dalai, and Janusz A Kozinski. Supercritical water gasification of biomass for hydrogen production. *International Journal of Hydrogen Energy*, 39(13):6912–6926, 2014.

[28] Liejin Guo, Yunan Chen, and Jiarong Yin. Organic waste gasification in near-and supercritical water. In *Application of Hydrothermal Reactions to Biomass Conversion*, pages 315–354. Springer, 2014.

[29] Y Guo, SZ Wang, DH Xu, YM Gong, HH Ma, and XY Tang. Review of catalytic supercritical water gasification for hydrogen production from biomass. *Renewable and Sustainable Energy Reviews*, 14(1):334–343, 2010.

[30] Douglas C Elliott. Catalytic hydrothermal gasification of biomass. *Biofuels, Bioproducts and Biorefining*, 2(3):254–265, 2008.

[31] Pooya Azadi and Ramin Farnood. Review of heterogeneous catalysts for sub-and supercritical water gasification of biomass and wastes. *International Journal of Hydrogen Energy*, 36(16):9529–9541, 2011.

[32] Thomas M Yeh, Jacob G Dickinson, Allison Franck, Suljo Linic, Levi T Thompson, and Phillip E Savage. Hydrothermal catalytic production of fuels and chemicals from aquatic biomass. *Journal of Chemical Technology and Biotechnology*, 88(1):13–24, 2013.

[33] Zhen Fang. *Near-critical and supercritical water and their applications for biorefineries*. Springer, Dordrecht, 2014.

[34] Jude A Onwudili. Hydrothermal gasification of biomass for hydrogen production. In *Application of Hydrothermal Reactions to Biomass Conversion*, pages 219–246. Springer, 2014.

[35] Chao He, Chia-Lung Chen, Apostolos Giannis, Yanhui Yang, and Jing-Yuan Wang. Hydrothermal gasification of sewage sludge and model compounds for renewable hydrogen production: A review. *Renewable and Sustainable Energy Reviews*, 39:1127–1142, 2014.

[36] Xiaodong Xu, Yukihiko Matsumura, Jonny Stenberg, and Michael Jerry Antal. Carbon-catalyzed gasification of organic feedstocks in supercritical water. *Industrial & Engineering Chemistry Research*, 35(8):2522–2530, 1996.

[37] Waldner. *Catalytic Hydrothermal Gasification of Biomass for the Production of Synthetic Natural Gas*. PhD thesis, ETH Zürich (CH), 2007.

[38] Hung Thanh Nguyen, Haimeng Lu, Eiichiro Kobayashi, Takahiro Ishikawa, and Masaharu Komiyama. Raney-nickel catalyst deactivation in supercritical water gasification of ethanol fermentation stillage and its mitigation. *Topics in Catalysis*, 57(10-13):1078–1084, 2014.

[39] Hideki Takahashi, Stanislav Kopriva, Mario Giordano, Kazuki Saito, and Rüdiger Hell. Sulfur assimilation in photosynthetic organisms: molecular functions and regulations of transporters and assimilatory enzymes. *Annual review of plant biology*, 62:157–184, 2011.

[40] Stanislav V Vassilev, David Baxter, Lars K Andersen, and Christina G Vassileva. An overview of the composition and application of biomass ash. part 1. phase–mineral and chemical composition and classification. *Fuel*, 105:40–76, 2013.

[41] Yan Zhou, Lance Schideman, Guo Yu, and Yuanhui Zhang. A synergistic combination of algal wastewater treatment and hydrothermal biofuel production maximized by nutrient and carbon recycling. *Energy & Environmental Science*, 6(12):3765–3779, 2013.

[42] Ting Cai, Stephen Y Park, and Yebo Li. Nutrient recovery from wastewater streams by microalgae: status and prospects. *Renewable and Sustainable Energy Reviews*, 19:360–369, 2013.

[43] Umakanta Jena, Nisha Vaidyanathan, Senthil Chinnasamy, and KC Das. Evaluation of microalgae cultivation using recovered aqueous co-product from thermochemical liquefaction of algal biomass. *Bioresource technology*, 102(3):3380–3387, 2011.

[44] BJ He, Y Zhang, TL Funk, GL Riskowski, Y Yin, et al. Thermochemical conversion of swine manure: an alternative process for waste treatment and renewable energy production. *Transactions of the ASAE*, 43(6):1827–1834, 2000.

[45] Chao Gai, Yuanhui Zhang, Wan-Ting Chen, Yan Zhou, Lance Schideman, Peng Zhang, Giovana Tommaso, Chih-Ting Kuo, and Yuping Dong. Characterization of aqueous phase from the hydrothermal liquefaction of chlorella pyrenoidosa. *Bioresource technology*, 2014.

[46] Laura Garcia Alba, Cristian Torri, Daniele Fabbri, Sascha RA Kersten, and Derk WF Wim Brilman. Microalgae growth on the aqueous phase from hydrothermal liquefaction of the same microalgae. *Chemical engineering journal*, 228:214–223, 2013.

[47] Douglas C Elliott, Todd R Hart, Andrew J Schmidt, Gary G Neuenschwander, Leslie J Rotness, Mariefel V Olarte, Alan H Zacher, Karl O Albrecht, Richard T Hallen, and Johnathan E Holladay. Process development for hydrothermal liquefaction of algae feedstocks in a continuous-flow reactor. *Algal Research*, 2(4):445–454, 2013.

[48] Douglas C Elliott, Todd R Hart, Gary G Neuenschwander, Leslie J Rotness, Guri Roesijadi, Alan H Zacher, and Jon K Magnuson. Hydrothermal processing of macroalgal feedstocks in continuous-flow reactors. *ACS Sustainable Chemistry & Engineering*, 2(2):207–215, 2013.

[49] Zhong Yi Ding, Michael A Frisch, Lixiong Li, and Earnest F Gloyna. Catalytic oxidation in supercritical water. *Industrial & Engineering Chemistry Research*, 35(10):3257–3279, 1996.

[50] Y Matsumura, X Xu, and MJ Antal. Gasification characteristics of an activated carbon in supercritical water. *Carbon*, 35(6):819–824, 1997.

[51] Michael Jerry Antal, Stephen Glen Allen, Deborah Schulman, Xiaodong Xu, and Robert J Divilio. Biomass gasification in supercritical water. *Industrial & Engineering Chemistry Research*, 39(11):4040–4053, 2000.

[52] Maurice H Waldner and Frédéric Vogel. Renewable production of methane from woody biomass by catalytic hydrothermal gasification. *Industrial & engineering chemistry research*, 44(13):4543–4551, 2005.

[53] Tylisha M Brown, Peigao Duan, and Phillip E Savage. Hydrothermal liquefaction and gasification of nannochloropsis sp. *Energy & Fuels*, 24(6):3639–3646, 2010.

[54] Microanalysis Laboratory. http://scs.illinois.edu/microanalysis/, (retrieved February 24, 2015).

[55] Agilent Technologies, Hydrogen Detection with a TCD using Mixed Carrier Gas on the Agilent Micro GC, http://www.chem.agilent.com/Library/applications/5991-3199EN.pdf (retrieved February 26, 2015).

[56] Swagelok. Gaugeable Tube Fittings and Adapter Fittings, http://www.swagelok.com/downloads/webcatalogs/En/ms-01-140.pdf (retrieved February 24, 2015).

[57] Emhemmed A Youssef, George Nakhla, and Paul A Charpentier. Co-gasification of catechol and starch in supercritical water for hydrogen production. *international journal of hydrogen energy*, 37(10):8288–8297, 2012.

[58] Takafumi Sato, Kentaro Inda, and Naotsugu Itoh. Gasification of bean curd refuse with carbon supported noble metal catalysts in supercritical water. *biomass and bioenergy*, 35(3):1245–1251, 2011.

[59] Aritomo Yamaguchi, Norihito Hiyoshi, Osamu Sato, and Masayuki Shirai. Gasification of organosolv-lignin over charcoal supported noble metal salt catalysts in supercritical water. *Topics in Catalysis*, 55(11-13):889–896, 2012.

[60] Emhemmed A Youssef, Elsayed Elbeshbishy, Hisham Hafez, George Nakhla, and Paul Charpentier. Sequential supercritical water gasification and partial oxidation of hog manure. *international journal of hydrogen energy*, 35(21):11756–11767, 2010.

[61] Material Safety Data Sheet - Manganese (IV) Dioxide, http://avogadro.chem.iastate.edu/MSDS/MnO2.htm (retrieved February 25, 2015).

[62] Douglas C Elliott, L John Sealock Jr, and Eddie G Baker. Chemical processing in high-pressure aqueous environments. 2. development of catalysts for gasification. *Industrial & Engineering Chemistry Research*, 32(8):1542–1548, 1993.

[63] Elie Afif, Pooya Azadi, and Ramin Farnood. Catalytic hydrothermal gasification of activated sludge. *Applied Catalysis B: Environmental*, 105(1):136–143, 2011.

[64] Martin Schubert. *Catalytic Hydrothermal Gasification of Biomass - Salt Recovery and Continuous Gasification of Glycerol*. PhD thesis, ETH Zürich (CH), 2010.

[65] Y Calzavara, C Joussot-Dubien, G Boissonnet, and S Sarrade. Evaluation of biomass gasification in supercritical water process for hydrogen production. *Energy Conversion and Management*, 46(4):615–631, 2005.

[66] Edgar Gasafi, Marion-Yvonne Reinecke, Andrea Kruse, and Liselotte Schebek. Economic analysis of sewage sludge gasification in supercritical water for hydrogen production. *Biomass and Bioenergy*, 32(12):1085–1096, 2008.